- 1 Epigenetic drift score captures directional methylation variability and
- 2 links aging to transcriptional, metabolic, and genetic alterations
- 3 Xiu Fan^{1, 2 #}, Qili Qian^{3, 4 #}, Wenran Li^{3, 4}, Tianzi Liu^{3, 4}, Changqing Zeng^{1, 2, 5}, Peilin Jia^{1, 2}, Huandong
- 4 Lin⁶, Xin Gao⁶, Li Jin^{4, 7}, Mingfeng Xia^{6*}, Sijia Wang^{3, 8*}, Fan Liu^{9, 1*}
- 5 1. China National Center for Bioinformation, Beijing, China.
- 6 2. Beijing Institute of Genomics, Chinese Academy of Sciences, Beijing, China.
- 7 3. CAS Key Laboratory of Computational Biology, Shanghai Institute of Nutrition and Health, University
- 8 of Chinese Academy of Sciences, Chinese Academy of Sciences, Beijing, China.
- 9 4. Collaborative Innovation Center of Genetics and Development, Fudan University, Shanghai, China.
- 5. Institute of Biomedical Research, Henan Academy of Sciences, Zhengzhou, China.
- 11 6. Department of Endocrinology and Metabolism, Zhongshan Hospital, Fudan Institute for Metabolic
- 12 Disease, Human Phenome Institute, Fudan University, Shanghai, China.
- 13 7. Human Phenome Institute, Zhangjiang Fudan International Innovation Center, and Ministry of
- 14 Education Key Laboratory of Contemporary Anthropology, Fulocal University, Shanghai, China.
- 15 8. Center for Excellence in Animal Evolution and Genetics, Chinese Academy of Sciences, Kunming,
- 16 China.

- 9. Department of Forensic Sciences, College of Criminal Justice, Naif Arab University for Security
- 18 Sciences, Riyadh, Kingdom Saudi Arabia.
- 20 # These authors contribute equally to this work
- * Correspondence: Fan Liu fliu@nauss.edu.sa, Sijia Wang wangsijia@picb.ac.cn, or Mingfeng Xia
- 22 <u>dr xiamingfeng@163.com</u>.

- 23 Running title: Epigenetic drift score captures directional methylation variability
- 24 Keywords: epigenetic drift; aging; lipoprotein metabolites; EWDS; GWAS
- 27 Authors' email addresses

- 28 Xiu Fan, <u>fanxiu2018d@big.ac.cn</u>
- 29 Qili Qian, qianqili@picb.ac.cn
- Wenran Li, <u>liwenran@picb.ac.cn</u>
- 31 Tianzi Liu, <u>Tzliu@sinh.ac.cn</u>
- 32 Changqing Zeng, czeng@big.ac.cn
- Peilin Jia, pjia@big.ac.cn
- Huandong Lin, <u>lin.huandong@zs-hospital.sh.cn</u>
- 35 Xin Gao, zhongshan endo@126.com
- 36 Li Jin, <u>lijin@fudan.edu.cn</u>
- 37 Mingfeng Xia, <u>dr xiamingfeng@163.com</u>
- 38 Sijia Wang, wangsijia@picb.ac.cn
- Fan Liu, fliu@nauss.edu.sa
- 40 Authors' ORCIDs
- 41 Xiu Fan, 0000-0002-8590-9859
- 42 Qili Qian, 0009-0005-8797-5242
- 43 Wenran Li, 0000-0002-1712-6895

- 44 Tianzi Liu, 0000-0002-7401-3571
- 45 Changqing Zeng, 0000-0002-0037-1771
- 46 Peilin Jia, 0000-0003-4523-4153
- 47 Huandong Lin, 0000-0002-4266-3799
- 48 Xin Gao, 0000-0003-1864-7796
- 49 Mingfeng Xia, 0000-0002-5650-0165
- 50 Sijia Wang, 0000-0001-6961-7867
- 51 Fan Liu, 0000-0001-9241-8161

Abstract

53

54

55

56

57

58

59

60

61

62

63

64

65

66

67

68

69

70

71

72

73

74

75

76

77

Epigenetic drift refers to the gradual and stochastic accumulation of epigenetic changes, such as DNA methylation variability, with advancing age. Although increasingly recognized for its potential role in aging biology, its extent, biological significance, and population specificity remain insufficiently characterized. Here, we present the first comprehensive epigenome-wide drift study (EWDS) in a large Chinese cohort (n = 3,538), with replication in two independent Chinese (total n = 1,467) and two European cohorts (total n = 956), to investigate the scale and relevance of epigenetic drift across populations. Through simulation, we identified White's test as the most powerful method among four alternatives for detecting age-associated methylation variability. Our EWDS revealed that 10.8% (50,385 CpGs) of sites on the 850K EPIC array exhibited epigenome-wide significant drift, with 99% showing increased inter-individual variability (positive drift) and 1% showing decreased variability (negative drift). Integration with single-cell RNA-seq data demonstrated that positive drift-CpGs are associated with increased transcriptional variability and upregulation in specific cell types, while negative drift-CpGs exhibit the opposite effect. We developed epigenetic drift scores (EDSs) to quantify individual drift burden; these scores are strongly age-associated and correlate with lipidomic profiles and clinical aging indicators. Longitudinal data confirm within-individual accumulation of drift over time. Finally, a GWAS of EDS identified genetic determinants of drift magnitude, including heritable loci (e.g., ASTN2, SOCS5). Collectively, these findings establish epigenetic drift as a pervasive, directional, and biologically meaningful feature of human aging.

Introduction

Epigenetic drift refers to the progressive, stochastic accumulation of molecular alterations across the epigenome during aging. These include changes in DNA methylation, histone modifications, chromatin remodeling, and non-coding RNAs. Collectively, such alterations disrupt gene regulatory networks, leading to transcriptional dysregulation, loss of cellular homeostasis, and increased vulnerability to agerelated diseases (Li and Tollefsbol 2016; López-Otín et al. 2023). Among these, DNA methylation drift

has emerged as the most extensively characterized component of epigenetic aging. It is typified by increased variance in methylation levels at specific CpG sites-termed drift-CpGs-over chronological age, distinguishing it from the linear age-associated methylation changes at epigenetic clock sites (Fraga et al. 2005; Horvath and Raj 2018; Seale et al. 2022). Importantly, epigenetic drift likely unfolds more gradually across wider temporal windows, capturing interindividual and cellular heterogeneity in a way that reflects biological aging beyond the linear progression captured by clock-based models. This stochastic accumulation is hypothesized to reflect rising intercellular and interindividual heterogeneity with age, potentially capturing biological aging more dynamically than static methylation clocks (Meyer and Schumacher 2024). Understanding and quantifying epigenetic drift may offer novel biomarkers for aging trajectories, disease susceptibility, and therapeutic interventions aimed at mitigating age-associated decline.

The etiology of epigenetic drift is multifactorial. Genetic predisposition accounts for substantial interindividual variation in baseline methylation patterns (Shah et al. 2014). In addition, longitudinal twin studies have underscored the influence of environmental factors; for instance, Tan et al. identified over 2,000 CpGs exhibiting significant methylation drift over a decade, strongly implicating environmental exposures (Tan et al. 2016). Infectious agents, such as cytomegalovirus, have also been shown to induce widespread methylation variance in a cell-composition-independent manner (Bergstedt et al. 2022). At the chromatin level, drift-CpGs are enriched in repressive Polycomb-bound regions (Slieker et al. 2016) and exhibit pronounced variability on the inactive X Chromosome (Liu et al. 2023), suggesting epigenomic compartmentalization of drift. The biological consequences of epigenetic drift are increasingly being explored. Hannum et al. showed that drift-CpGs in blood are associated with transcriptional changes, implicating drift as a potential regulator of aging pace (Hannum et al. 2013). At the molecular level, this may manifest as altered transcriptional output and increased expression noise, disrupting cellular function.

Detecting epigenetic drift, however, requires robust statistical modeling capable of detecting changes in variance rather than mean methylation. Several approaches have been proposed. The most commonly used methods apply heteroscedasticity tests, such as the Breusch–Pagan test or double generalized linear

models (DGLMs), to identify CpG sites whose methylation variance increases linearly with age (Slieker et al. 2016; Bergstedt et al. 2022; Liu et al. 2023). Complementary entropy-based metrics estimate methylome-wide disorder, capturing the global stochasticity of the epigenome (Hannum et al. 2013; Wang et al. 2024). These statistical frameworks serve as critical tools for identifying drift-CpGs and quantifying the systemic erosion of epigenetic fidelity.

Despite recent advances, several key challenges remain. First, there is no consensus on the optimal statistical framework for identifying drift-CpGs, with different studies applying distinct models and yielding limited concordance. Second, the generalizability of previously identified drift-CpGs is limited, as most were derived in European populations and lack validation across diverse ancestries, such as East Asians. Third, previous research has predominantly focused on positive drift, CpGs with increasing methylation variance over age, while negative drift-CpGs remain largely understudied, despite their potential biological importance. Fourth, it is still unclear whether drift-CpGs are cell-type specific or reflect a shared aging signature across hematopoietic lineages. Fifth, although entropy-based metrics have been used to estimate global methylation disorder, no standardized method currently exists to construct an epigenetic drift score (EDS) at the individual level using a finite set of CpGs. Lastly, the biological relevance of drift-CpGs, particularly their contribution to age-related complex traits, and their relationship with underlying genetic architecture, remains poorly understood.

To address these challenges, we first performed a comprehensive evaluation of four commonly used statistical methods for identifying drift-CpGs, using both computer simulations and empirical population data. We then applied this method to 735,267 CpG sites (850K EPIC Array) measured in 3,538 Chinese individuals, systematically identifying a high-confidence set of drift-CpGs. Our replication analysis was conducted in 2,423 individuals from two additional Chinese cohorts and two European cohorts. Both positive and negative drift-CpGs were characterized to reveal complementary biological patterns. We further investigated whether drift-CpGs exhibit cell-type specificity or represent shared signatures of hematopoietic aging by integrating single cell RNA-seq analyses. To quantify individual-level epigenetic drift, we developed an EDS based on a finite subset of drift-CpGs, offering a standardized alternative to

entropy-based metrics. Finally, we evaluated the functional relevance of EDS through association analyses with age, lipidomic profiles, and genome-wide genetic variation, uncovering potential mechanistic links between stochastic epigenetic changes and age-related complex traits.

Results

Population characteristics

An overview of the study design, detection technologies, and analytical workflow is presented in Fig. 1. The discovery cohort, the National Survey of Physical Traits (NSPT), comprised 3,538 Chinese individuals with a mean age of 50.2 years (SD = 12.7, range 18-83) and 37.0% male participants (Supplemental Table S1). The first replication cohort included 1,060 individuals from the Chinese Academy of Sciences cohort (CAS), predominantly highly educated individuals in intellectual professions, with a mean age of 40.8 years (SD = 9.4, range 22-64) and 59.7% male participants. The second replication cohort, a longitudinal study from the Shanghai Changfeng Study (Changfeng), spanned a median follow-up period of 4 years with 407 subjects. Baseline ages ranged from 47.6 to 80.0 years, with a mean age of 61.4 years (SD = 7.4), and follow-up ages ranged from 51.9 to 84.0 years, with a mean age of 65.5 years (SD = 7.3). DNA methylation at 735,267 CpGs, overlapping between the discovery and replication cohorts, showed highly concordant distributions (Supplemental Fig. S1). For subsequent epigenome-wide analysis, we retained 469,061 CpGs after excluding those affected by mQTLs (Peng et al. 2024), those with minimal variance in age-regressed residuals ($R^2 < 1 \times 10^{-5}$), or those significant in a multimodal distribution test ($p < 1 \times 10^{-4}$).

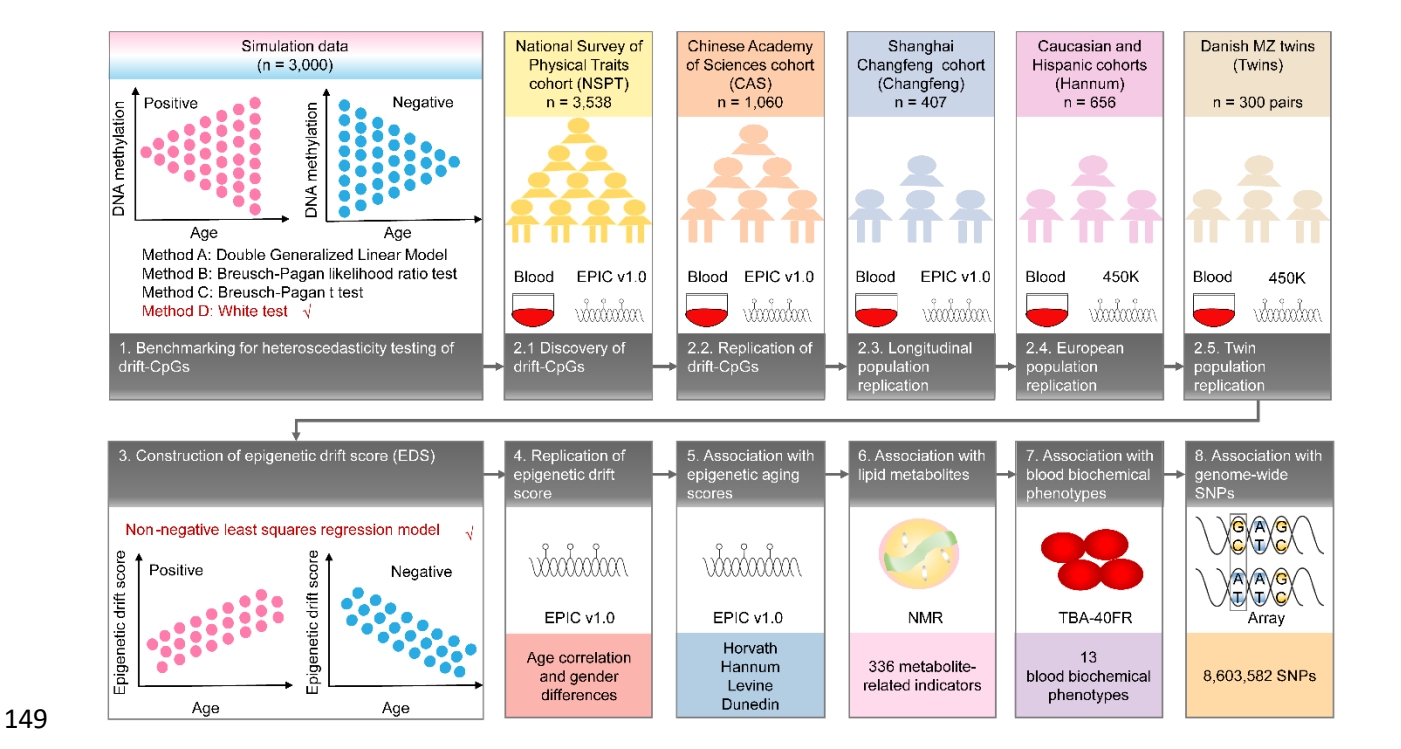


Figure 1. Schematic representation of the study design, detection technologies, and analytic approaches. The method marked in red text and with a checkmark ($\sqrt{}$) was selected for downstream analysis.

Positive and negative drifts enriched in different functional regions

A simulation analysis was conducted to compare the statistical power and type-I error rates of four existing heteroscedasticity test methods: method A: double generalized linear model (Liu et al. 2023), method B: Breusch-Pagan likelihood ratio based chi-square statistic (Bergstedt et al. 2022), method C: Breusch-Pagan *T*-statistic (Slieker et al. 2016), and method D: White Test (White 1980) (see Supplementary Methods for details). This analysis showed that method B was overly aggressive, while method A was overly conservative. Method D showed superior performance in scenarios involving non-linear relationships between CpG variance and age (Supplemental Fig. S2). Using White Test, EWDS identified 10.8% of CpG sites (50,385) as drift-CpGs (p<1×10⁻⁷, Fig. 2A, B). This number significantly exceeds findings from previous studies, including one involving 385 Swiss twin pairs using the 450K array, which identified 571 drift-CpGs (different method due to twin samples), with 229 overlapping with

our list (Wang et al. 2018). Another study of 3,295 European individuals from the BIOS Consortium using the 450K array and the Method C identified 6,366 drift-CpGs (Fig. 2C), with 3,000 overlapping with ours (Wang et al. 2018). Our number also surpassed that from The Milieu Intérieur study of 968 Europeans (Bergstedt et al. 2022), which identified 20,140 drift-CpGs from a total of 644,517 CpGs using Method B. These discrepancies are likely attributable to a combination of factors such as larger sample size, broader age range, greater CpG coverage, and enhanced statistical power. The vast majority of the identified drift-CpGs (99.0%, n=49,877) exhibited an increase in variance with aging, termed as positive drift-CpGs (Fig. 2D), while a small fraction showed a significant decrease in variance, termed as negative drift-CpGs (n=508, 1.0%, Fig. 2E). Positive drift-CpGs were highly significantly enriched in expression-repressed CpG islands (CGIs) (OR=2.4, p<1×10⁻³⁰⁰, Fig. 2F, G), whereas negative drift-CpGs were significantly enriched in expression-active non-CGIs, such as open sea regions (OR = 2.4, p<8.8×10⁻¹⁹), with a particularly pronounced enrichment in enhancers (OR=10.1, p =2.1×10⁻⁶⁴). A transcription factor binding motif enrichment analysis showed that negative drift-CpGs significantly enriched at *AHR-ARNT*, *CREB3L4*, and *GMEB2* (Supplemental Fig. S3).

Compared to the abundant age-associated CpGs identified by linear regression in the same dataset, referred to here as clock-CpGs (31.2%, n = 146,497, $p < 1 \times 10^{-7}$), the number of drift-CpGs was substantially smaller and exhibited lower statistical significance, as expected. Nonetheless, we observed a significant overlap between drift-CpGs and clock-CpGs (23.3%, n = 34,118), indicating that methylation drift and directional age associations are not mutually exclusive. In fact, drift-CpGs were significantly more likely than non-drift CpGs to also exhibit age-associated mean changes in methylation (OR = 5.7, $p < 1 \times 10^{-300}$, Supplemental Table S2). Notably, positive drift-CpGs were more frequently associated with CpGs that also showed increasing average methylation with age (positive clock-CpGs), whereas negative drift-CpGs were more likely to coincide with CpGs that decreased in methylation with age (negative clock-CpGs, OR = 1.3, $p = 7.8 \times 10^{-3}$, Supplemental Table S2). Positive drift-CpGs and positive clock-CpGs were most significantly enriched in CGI Islands (Fig. 2H), while negative drift-CpGs and negative

clock-CpGs were most significantly enriched in enhancers (Fig. 2I). This concordance suggests a partial coupling between directional epigenetic aging and increased epigenetic variability.

We examined whether changes in DNA methylation variance at CpG sites are associated with initial (young group age < mean - 2SD) and terminal (old group age > mean + 2SD) methylation levels. Specifically, we asked whether reduced variance indicates convergence toward methylation extremes (0 or 1), and whether increased variance reflects divergence from such states. This analysis identified differential drift patterns based on the direction of methylation drift (Fig. 2J-L). Positive drift-CpGs predominantly remained at intermediate methylation ranges (0.1-0.9) throughout aging, rarely converging toward either hypermethylation or hypomethylation extremes. In contrast, negative drift-CpGs typically moved from intermediate methylation states toward methylation extremes but rarely vice versa. These observations suggest fundamentally different biological mechanisms underlying positive versus negative methylation drift during aging. We hypothesis that negative drift, characterized by shifts towards methylation extremes, likely reflects more targeted biological aging processes such as cellular senescence or clonal expansions, whereas positive drift might represent broader stochastic or heterogeneous aging processes.

Epigenetic drift's cell-type specificity and transcriptional impact

To investigate whether epigenetic drift-CpGs are driven by changes in blood cell-type composition, we applied the EpiDISH algorithm (Teschendorff and Zheng 2017). Among the 50,385 identified drift-CpGs, the majority (88%) did not exhibit cell-type-specific methylation patterns, suggesting that most epigenetic drift occurs independently of blood cell composition (Fig 2M). Of the 6,226 CpGs (12%) that did show significant cell-type-specificity, the vast majority (>99%) were associated with lymphoid lineage cells. Specifically, these CpGs were predominantly enriched in B cells (82%), followed by CD8⁺ T cells (12%), CD4⁺ T cells (4%), and natural killer (NK) cells (2%), while less than 1% were linked to myeloid cells. Importantly, CD4⁺ T cell-specific drift-CpGs (n=266) showed a distinct pattern, all of which exhibited negative drift with age. These findings suggest a cell-type-specific suppression of epigenetic drift noise in

CD4⁺ T cells, in contrast to the general age-associated increase observed in other cell types.

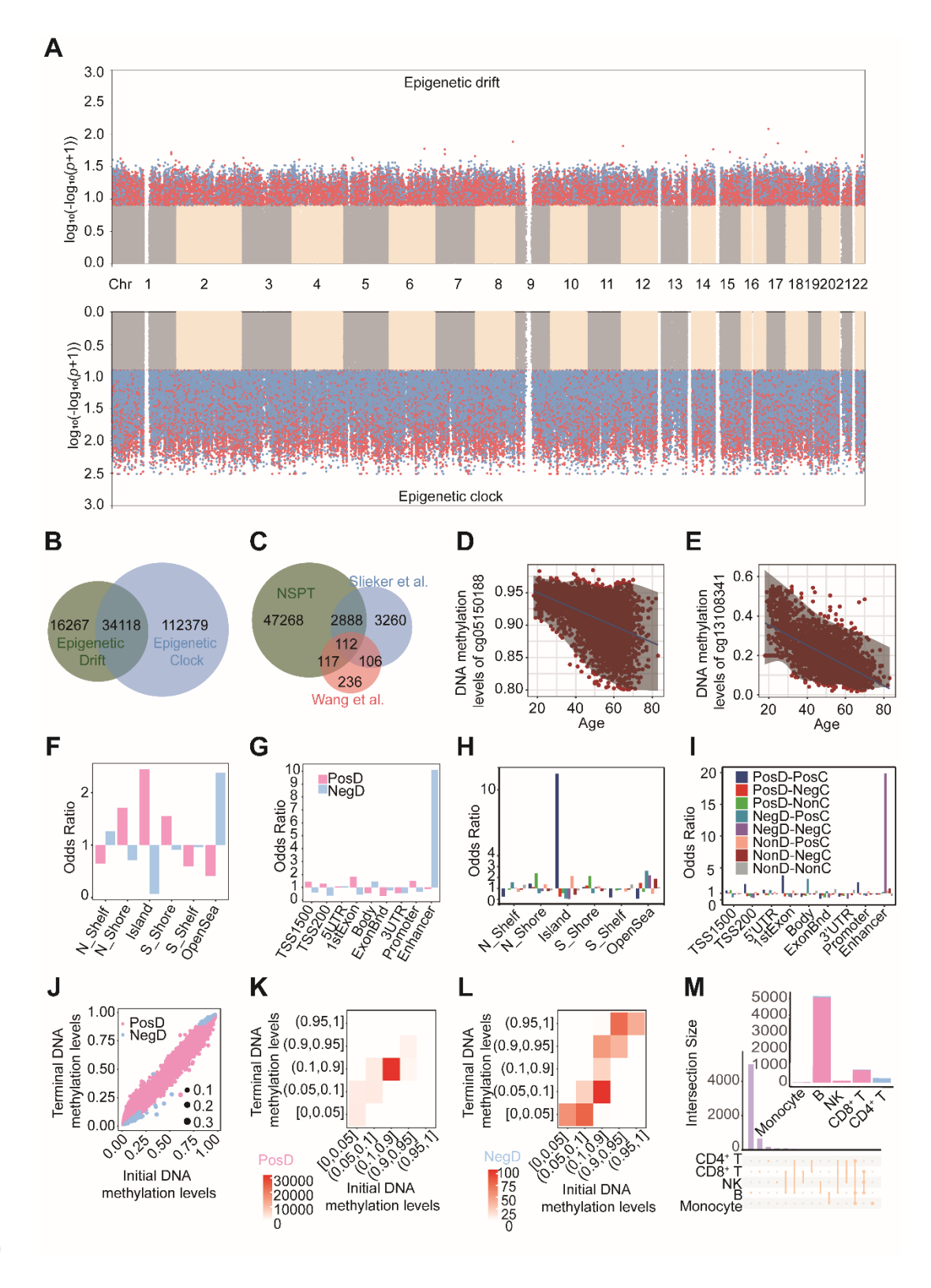
Representative examples of lymphoid-, myeloid-, and CD4⁺ T cell-specific drifts are provided in Supplemental Fig. S4A–C.

To investigate how age-associated DNA methylation drift influences gene expression, we integrated drift-CpG profiles with single-cell RNA sequencing (scRNA-seq) data across peripheral blood mononuclear cell (PBMC) immune cell types. Our analysis revealed statistically significant, albeit modest, shifts in gene expression profiles associated with drift-CpGs relative to the genome-wide background (Supplemental Fig. S5A-B). Specifically, genes associated with positive drift-CpGs exhibited a tendency towards higher mean expression and discernibly greater expression variability compared to the genome-wide background, suggesting a relatively more active yet potentially unstable transcriptional state. Conversely, genes adjacent to negative drift-CpGs displayed slightly but significantly lower transcriptional noise, indicating a more stable transcriptional pattern.

We further examined age-related transcriptional changes in immune cells. Although overall mean transcriptional activity showed a modest but significant increase in older individuals (Supplemental Fig. S5A–B), stratifying by drift direction revealed consistent, albeit subtle, age-associated increases in transcriptional levels for genes proximal to both positive and negative drift-CpGs. Notably, only genes near positive drift-CpGs showed increased transcriptional variance with age, while those near negative drift-CpGs did not.

Subsequent cell-type-specific analyses confirmed that age-related transcriptional changes associated with drift-CpGs were largely non-overlapping across immune cell types, underscoring a high degree of cell-type specificity (Supplemental Fig. S5C-F). In CD4⁺ T cells, BASiCS analysis revealed reduced transcriptional noise in aged individuals for genes associated with positive drift-CpGs, suggesting a context-dependent noise-suppressive function. The most pronounced transcriptional perturbations in genes associated with positive epigenetic drift were observed in B cells (Supplemental Fig. S5G).

Conversely, negative epigenetic drift primarily affected CD4⁺ T cells, driving distinct transcriptional changes in this subset (Supplemental Fig. S5H).



242

243

244

245

246

247

248

249

250

251

252

253

254

255

256

257

258

259

260

261

262

263

264

Figure 2. Epigenome-wide identification and annotation of drift- and clock-CpGs. A, Manhattan plot of significant CpGs ($p < 1 \times 10^{-7}$), colored by drift (blue), clock (blue), or both (red) effects. B, Venn diagram showing overlap between drift- and clock-CpGs; C, Overlap of NSPT drift-CpGs with those from Slieker et al. and Wang et al. **D**–**E**, Representative CpGs with age-related increase (D) or decrease (E) in methylation variance. F-G, Genomic enrichment of positive and negative drift-CpGs (F: CpG island-related; G: gene-related features). H-I, Genomic enrichment of drift- and clock-CpGs (H: CpG island-related; I: gene-related features). J, Scatter plot of initial (young) vs. terminal (old) methylation levels at drift-CpGs. K-L, Heatmaps of positive (K) and negative (L) drift-CpG distribution by methylation levels. M, Upset plot showing cell-type specificity of drift-CpGs across immune lineages. Abbreviations: PosD, positive drift-CpGs; NegD, negative drift-CpGs; PosC, positive clock-CpGs; NegC, negative clock-CpGs; NonD, non-drift CpGs; NonC, non-clock CpGs. Robust drifts in an independent CAS cohort In the CAS cohort of 1,060 samples, 48,171 CpGs overlapped with the 50,385 significant CpGs identified in NSPT. Of these overlapping CpGs, 50.2% were replicated at a nominal significance level in CAS (p <0.05, OR = 8.9, fisher.test, $p < 2.2 \times 10^{-16}$, Fig. 3A, Supplemental Table S3). An analysis of these replicated drifts revealed that 99.9% of positive drifts were consistently positive, and 99.1% of the negative drifts remained negative. When applying more stringent significance criteria in the discovery cohort, we observed a progressive increase in replication rates, peaking at 100% for a threshold of 1×10⁻ ²⁰. Notably, both positive and negative drifts exhibited complete consistency at these stringent levels. In the CAS cohort, the most significantly replicated positive drift was observed on Chr4 for cg24035745 in FBXO2 (NSPT $p=5.1\times10^{-14}$, CAS $p=6.8\times10^{-11}$). Young individuals exhibited significantly smaller variance in methylation compared to mid-aged and elderly individuals (Fig. 3B). Increased

expression of FBXO2 occurs with neurons developmental maturation (Ciceri et al. 2024). FBXO2

deficiency exacerbated deficits in motor function, and enhanced neurodegeneration(Liu et al. 2020).

266

267

268

269

270

271

272

273

274

275

276

277

278

279

280

281

282

283

284

285

286

287

288

289

Similarly, the most significantly replicated negative drift was identified on Chr14 for cg13868026 in EVL (NSPT $p=6.8\times10^{-59}$, CAS $p=8.8\times10^{-7}$). In this case, young and mid-aged individuals showed significantly larger variance in methylation compared to elderly individuals (Fig. 3C). DNA methylation of EVL was identified a prognostic signature in colon cancer, and promoter methylation of EVL differs between individuals and between regions of the normal colon (Yi et al. 2011). The CAS cohort also replicated the presence of other top significant negative drift-CpGs that were found in or near MAPRE2, ARPIN-AP3S2, TRAPPC9, APBB1IP and FOXK1. Among these, methylation of FOXK1 has a known effect on the regulation of immune and metabolic functions (Fujinuma et al. 2023). Epigenetic drifts in independent longitudinal Changfeng population We further analysed the CAS-replicated drift-CpGs (23,758 out of the available 24,161) within the Changfeng longitudinal cohort to determine if the methylation levels showed any drift over an approximate follow-up period of 4 years. For each individual CpG site, we performed a paired t-test. This test compared the absolute deviation of the methylation level from the population mean at the baseline to the same deviation at the follow-up. In mathematical terms, it involved comparing |cpg - mean(cpg)| at baseline with those at follow-up. Our results indicated that 48.1% of the examined drift-CpGs exhibited a nominally significant difference (n=11,422, p<0.05, OR = 5.0, fisher.test, p < 2.2×10⁻¹⁶) between these two time points. Among these nominally significant CpGs, 99.7% exhibiting the same effect directions as observed in NSPT and CAS (Fig. 3D). These findings demonstrated the robustness of the drift effects at our identified sites and underscore the genuine impact of negative drifts. In Changfeng, the most significantly replicated positive drift-CpG was cg27099280 in CELF6 ($p = 6.2 \times 10^{-19}$, Fig. 3E) and negative drift-CpG was cg03883331in ZBTB18 ($p = 4.0 \times 10^{-4}$, Fig. 3F) and cg22005677 in LPP (p =0.02). The repeated highlighting of the negative drift at LPP in both the CAS and Changfeng cohorts underscores its robustness and prominence in our findings. It is important to note that both the CAS and Changfeng replication cohorts have narrower age ranges compared to the discovery cohort, which may

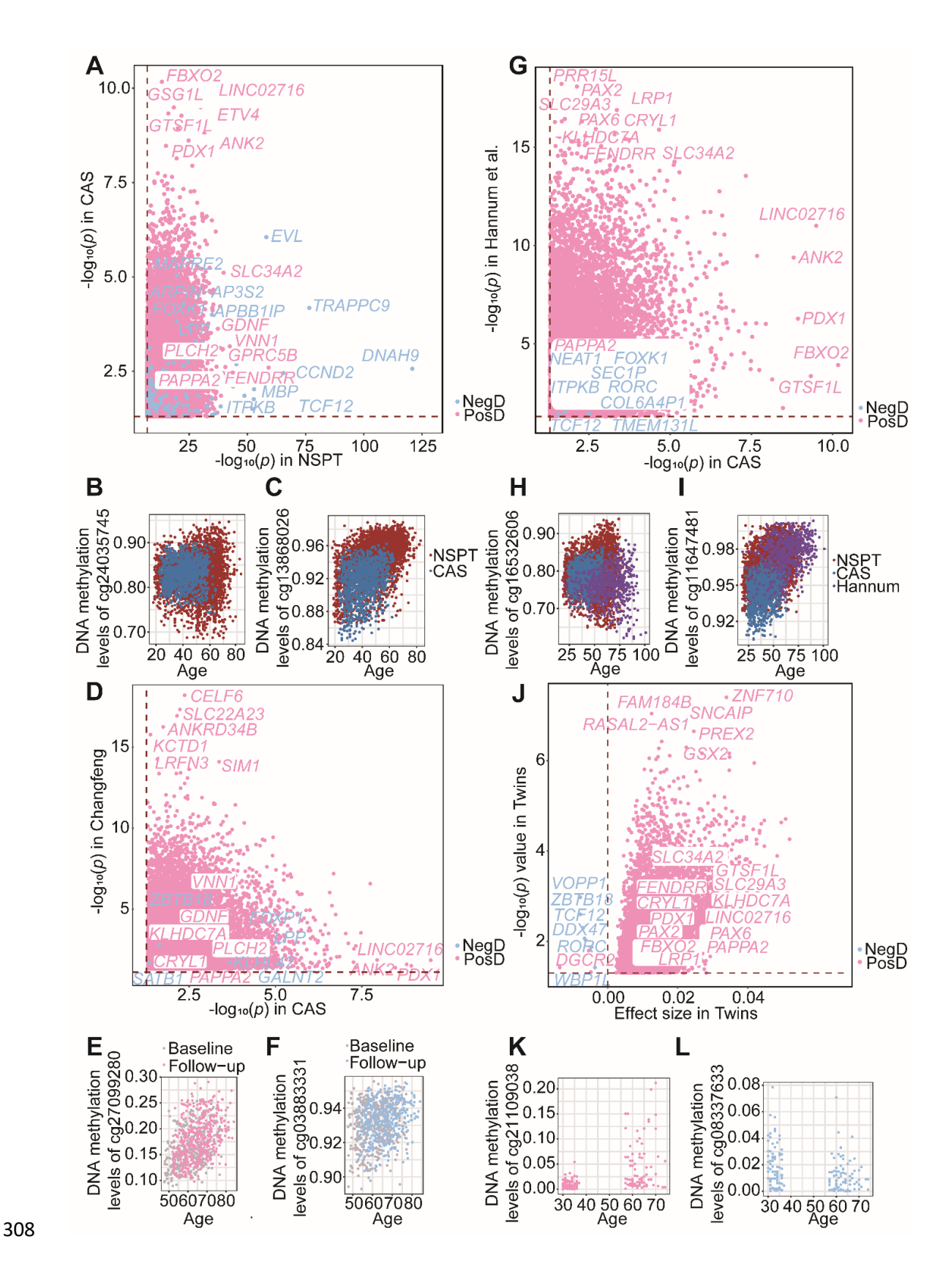
contribute to conservative replication rates. Functionally, the CpG site in ZBTB18 is instrumental in

regulating the expression of *ZBTB18*, a colorectal tumor suppressor gene(Bazzocco et al. 2021). Loss of its activity enhances chromatin accessibility and transcriptional adaptations that promote the phenotypic changes required for metastasis (Wang et al. 2023). This suggests that negative drifts may be involved in regulating global chromatin accessibility dysregulation in the development of age-related phenotypes.

Epigenetic drift is cross-ethnic

We further examined 14,909 of our drift-CpGs overlapping with the 450K beadchip in the dataset of Hannum et al. (Hannum et al. 2013), which consisted of a mixed population of 426 Caucasian and 230 Hispanic individuals (age range: 19-101 years). A substantial proportion (76.3%, 11,378 out of 14,909) exhibited nominally significant drifting effects in the same direction (OR = 9.3, fisher.test, $p < 2.2 \times 10^{-16}$, Fig. 3G, H, I).

Next, we focused on a cohort of 150 pairs of monozygotic (MZ) Danish twins aged 30 to 74 years (78 male pairs and 72 female pairs) (Tan et al. 2014). Our aim was to determine whether our identified drift-CpGs could account for previously observed inter-individual epigenetic variations (Planterose Jimenez et al. 2021). To this end, we categorized the MZ twins into two age groups (< 50 years and \ge 50 years). Using a *t*-test, we examined the absolute methylation level discrepancies (|MZ1 - MZ2|) between the two age groups. Among the CpGs corresponding with our drift-CpGs, a substantial proportion (49.6%, 6,731 out of 13,571) showed nominally significant drift effects (Fig. 3J, K, L). These findings support our hypothesis that aging plays a pivotal role in the epigenomic differentiation of MZ twins.



310

311

312

313

314

315

316

317

318

319

320

321

322

323

324

325

326

327

328

329

330

331

332

333

334

Figure 3. Replication of drift-CpGs in independent cohorts. A, Replication of significant drift-CpGs in CAS, with thresholds corresponding to Bonferroni significance in NSPT and nominal significance in CAS. CpGs are colored by drift direction and selected genes are labeled. **B–C**, Scatter plots of top positive (B: cg24035745) and negative (C: cg13868026) drift-CpGs validated in CAS. **D-F**, Validation of drift-CpGs in the Changfeng cohort, including representative positive (E: cg27099280) and negative (F: cg03883331) examples. G-I, Replication in Hannum et al., with representative positive (H: cg16532606) and negative (I: cg11647481) drift-CpGs. J-L, Validation in monozygotic Danish twins, including top positive (K: cg21109038) and negative (L: cg08337633) drift-CpGs. Abbreviations: PosD, Positive drift-CpGs; NegD, Negative drift-CpGs. Positive drifts related to neural system functions and negative drifts linked to immune functions GO and KEGG functional enrichment analyses of our replicated drift-CpGs have illuminated possible mechanisms tied to both positive and negative epigenetic drift (Fig. 4). Specifically, positive drift-CpGs (n=24,051) were markedly enriched for processes related to nervous system development ($p=7.9\times10^{-41}$ after FDR) and neuroactive ligand-receptor interaction ($p=6.2\times10^{-23}$ after FDR), corroborating Slieker et al.'s work (Slieker et al. 2016). Conversely, negative drift-CpGs (n=110) showed distinct enrichment in alpha-beta T cell differentiation ($p=1.4\times10^{-3}$ after FDR). Phenotype enrichment analysis, derived from EWAS Atlas data, revealed that positive drift-CpGs were significantly associated with phenotypes such as B Acute Lymphoblastic Leukemia ($p=1.8\times10^{-91}$ after FDR), hepatocellular carcinoma ($p<3.4\times10^{-39}$ after FDR), and Helicobacter pylori infection ($p=5.4\times10^{-38}$ after FDR). This finding aligns with earlier studies showing that increased DNA methylation variability frequently occurs at loci related to malignancy and can be predictive of cancer emergence(Landau et al. 2014; Feinberg and Levchenko 2023). In contrast, the phenotype enrichment for negative drift underscored aging as the most significantly associated trait $(p=1.3\times10^{-36} \text{ after FDR})$, followed by Down syndrome as the second most significant $(p=2.1\times10^{-24} \text{ after})$ FDR). These patterns suggest a differential impact of positive versus negative drift on phenotype expression, with negative drift showing a pronounced association with aging processes.

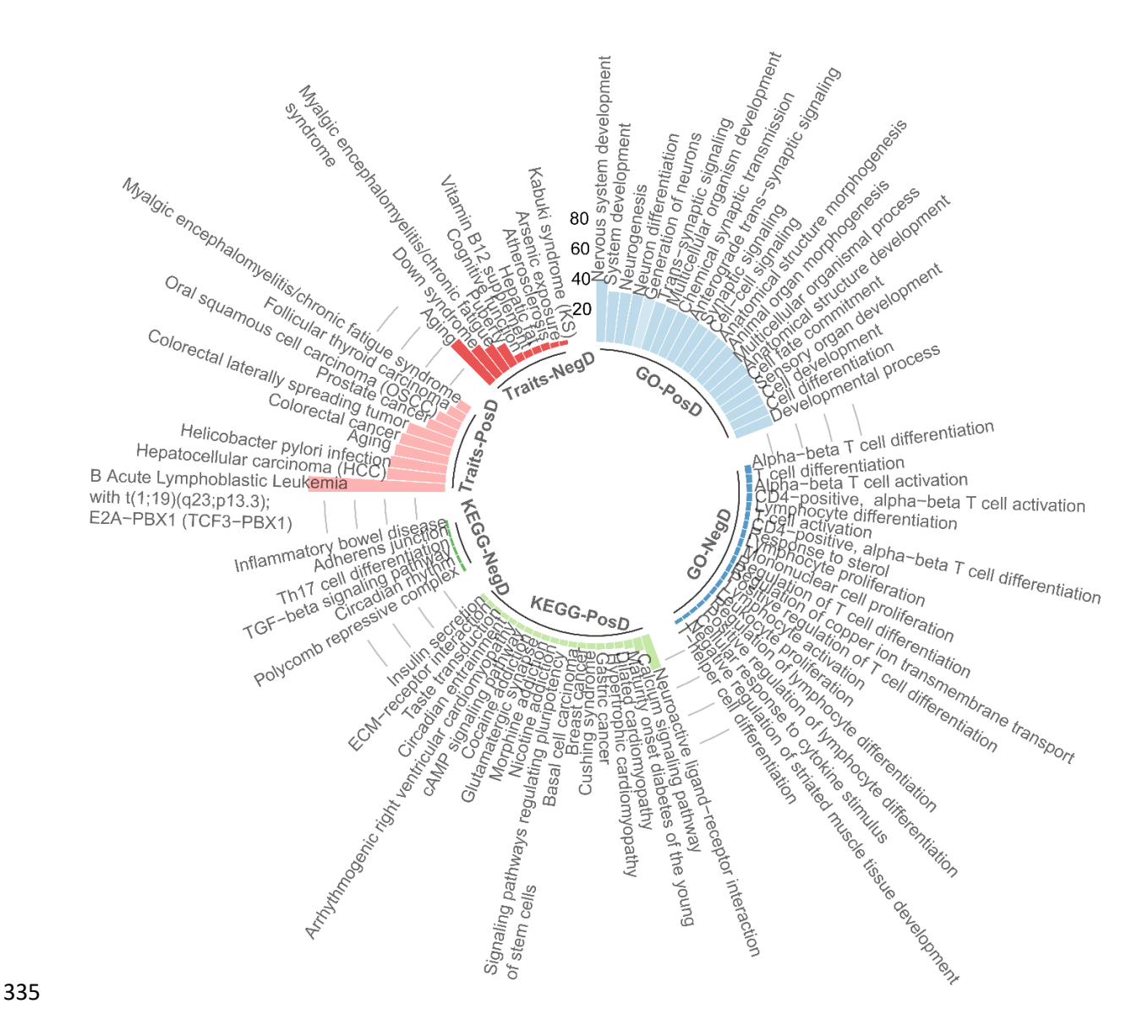


Figure 4. Biological and trait enrichments of directional epigenetic drift. This circular plot visualizes Gene Ontology (GO) terms, KEGG pathways, and traits enriched for positive (PosD) and negative (NegD) drift-CpGs. Enrichment score, calculated as $-\log_{10}(\text{FDR }p)$, increases with distance from center.

EDS represents a unique aging dimension

We developed a positive epigenetic drift score (EDS_POS) using 204 independent CpGs, each more than 500 kbp apart (Supplemental Table S4). These CpGs were selected from the 49,877 positive drift-CpGs identified in NSPT, based on their smallest Fisher combined p-values across NSPT, CAS, and Hannum et al., using a non-negative least squares regression model.

The EDS_POS ranges from 0 to 1, reflecting low to high levels of epigenetic positive drift. In both NSPT and Hannum et al., the distribution of EDS_POS was slightly right-skewed, with a mean of 0.41 (boxplot: 0.21, 0.32, 0.39, 0.47, 0.69). EDS_POS exhibited a linear correlation with age, which strengthened as more CpGs were included. Specifically, Pearson's correlation increased from 0 to 0.56 as the number of CpGs grew from 1 to 100, plateaued at 0.60 with 200 CpGs (Fig. 5A, B). The EDS_POS constructed in CAS using the same weights also demonstrated a highly consistent distribution (mean 0.39, boxplot: 0.25, 0.34, 0.37, 0.43, 0.56, Fig. 5C) and a robust age correlation (r = 0.50).

We also found that EDS_POS increases more slowly with age in females compared to males ($p = 3.7 \times 10^{-7}$, Fig. 5B). We then compared the performance of EDS_POS with a more robust but less sensitive score that included more CpGs with equal weights (11,367 positive drift-CpGs nominally replicated in both CAS and Hannum et al.). This score had a lower correlation with age (r = 0.46) than EDS_POS, likely due to added noise from less significant CpGs given equal weight. However, EDS_POS still showed a high correlation (r = 0.82) with this score (Fig. 5D). This result, along with the observation that age correlation plateaued after including 200 CpGs in EDS_POS, suggests that our EDS_POS effectively captures genome-wide epigenetic drift, with 204 drift-CpGs being sufficient for this purpose.

We similarly developed a negative epigenetic drift score (EDS_NEG) based on 81 significant negative drift-CpGs identified in NSPT. The EDS_NEG ranges from 0 to 1, indicating low to high levels of negative drift (Supplemental Table S5). In NSPT, the distribution of EDS_NEG was slightly right-skewed with a mean of 0.36 (boxplot: 0.23, 0.31, 0.36, 0.42, 0.57). EDS_NEG showed an increasingly strong negative correlation with age as more CpGs were included, reaching -0.38 when all 81 CpGs were included (r = -0.39 in males and r = -0.38 in females, Fig. 5E, F). The EDS_NEG constructed in CAS using the same weights demonstrated a highly consistent distribution (mean 0.42, boxplot statistics: 0.14, 0.31, 0.40, 0.50, 0.79, Fig. 5G) and a robust correlation with age (r = -0.49). A more robust but less sensitive score, based on 508 equally weighted negative drift-CpGs, also showed a negative correlation with age at -0.34. The correlation between EDS_NEG and this 508-CpG score was 0.54 (Fig. 5H).

We further investigated into the correlations of our EDS with several previously established DNA methylation-based aging scores, including Horvath (Horvath 2013), Hannum (Hannum et al. 2013), Levine (Levine et al. 2018), and Dunedin (Belsky et al. 2020) (Fig. 51). The Horvath and Hannum scores represent different versions of epigenetic clocks, while the Levine and Dunedin scores focus more on aging and aging pace. Our hypothesis posits that epigenetic drift may reflect a distinct or complementary aspect of aging compared to other epigenetic aging scores. Indeed, in NSPT, we observed expected modest levels of correlations prior to adjusting for age (EDS_POS: 0.29~0.63, EDS_NEG: -0.11~-0.39, Fig. 5J), which were further reduced after adjusting for age (EDS_POS: 0.17~0.31, EDS_NEG: -0.05~-0.09, Fig. 5K). These results support our hypothesis that epigenetic drift captures aging across different dimensions and scales compared to other epigenetic scores. Note that the methylation changes associated with epigenetic drift occur over much longer timescales, typically spanning decades, in contrast to the changes observed in epigenetic clock-CpGs, which often occur within a span of several years (Supplemental Fig. S6). Consequently, the EDS and the clock score may be capturing different aspects of aging, which could explain why the EDS exhibits a lower correlation with age compared to the typically high correlation (over 0.9) observed with clock scores.

In the NSPT cohort, individual-level entropy measures showed significant age associations: positive drift entropy significantly correlated with chronological age (Pearson's correlation coefficient, r = 0.39, $p = 6.9 \times 10^{-154}$) and negative drift entropy exhibited a significant inverse relationship (Pearson's correlationcoefficient, r = -0.51, $p = 8.5 \times 10^{-237}$, Fig. 5L-M). We observed moderate but significant concordance between individual entropy and population-level drift scores (Pearson's correlation coefficient, EDS_POS: r = 0.25, $p = 1.0 \times 10^{-61}$; negative: r = 0.29, $p = 6.7 \times 10^{-70}$). Furthermore, longitudinal analysis in the Changfeng cohort revealed a significant increase in overall epigenetic entropy over four years (paired *t*-test, $p = 1.7 \times 10^{-13}$), with the mean epigenetic entropy increasing from 4,101 at baseline to 4,172 at the 4-year follow-up, confirming the progressive nature of epigenetic drift at the individual level (Fig. 5N).

To evaluate EDS dynamics in the same individual's longitudinal aging process, we compared EDS_POS changes in methylation levels and variance from baseline to follow-up using longitudinal Changfeng data. These changes were then compared to analogous changes derived from a bootstrapped genome background, matched for the number of CpGs. The mean methylation ($p=3.6\times10^{-10}$) and variance ($p=2.8\times10^{-9}$) of these 204 positive drift-CpGs showed a statistically significant increase from baseline to the follow-up period (Fig. 5 O-P). Applying the weights derived from the NSPT to Changfeng confirmed a significant increase in EDS from the baseline to follow-up (baseline mean EDS=0.35; follow-up mean EDS=0.38, $p=1.2\times10^{-12}$, Fig. 5Q).

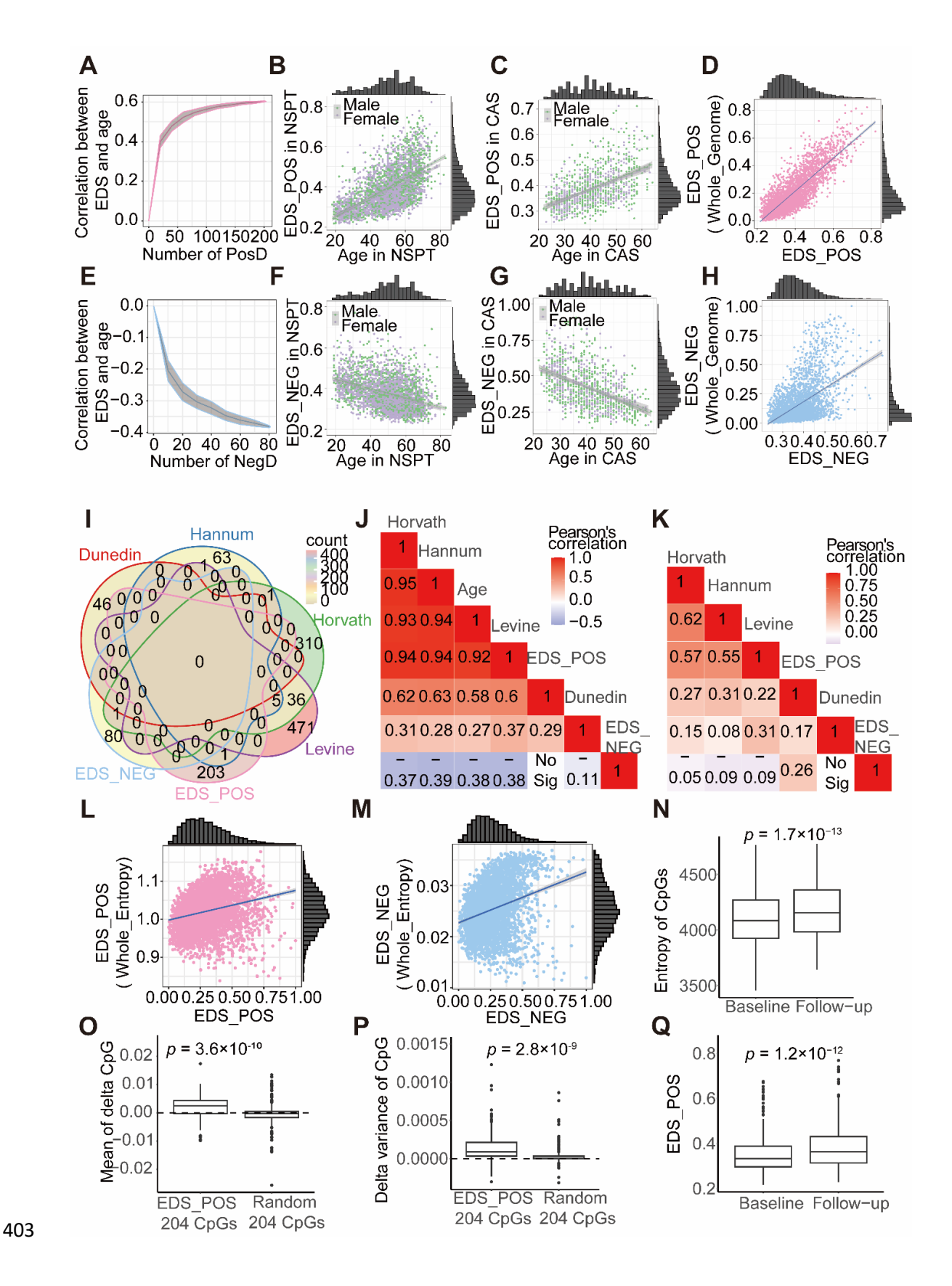


Figure 5. Validation and aging associations of the Epigenetic Drift Score (EDS). A, EDS_POS shows increasing correlation with age as more positive drift-CpGs are included. B–C, Scatter plots of EDS_POS vs. age in NSPT (B) and CAS (C), colored by gender. D, EDS_POS significantly correlates with genome-wide positive EDS. E–G, EDS_NEG similarly shows increasing age correlation (E) and gender-stratified associations in NSPT (F) and CAS (G). H, EDS_NEG correlates with genome-wide negative EDS. I, Venn diagram showing CpG overlap between EDS and four aging clocks. J–K, Heatmaps of correlations among EDS, aging clocks, and age, before (J) and after (K) age adjustment. L–M, EDS_POS (L) and EDS_NEG (M) correlate with genome-wide methylation entropy. N, Methylation entropy increases longitudinally over 4 years. O–Q, EDS_POS CpGs show greater increases in methylation mean (O), variance (P), and EDS score (Q) over time compared to random CpGs.

EDS associated with lipid metabolites

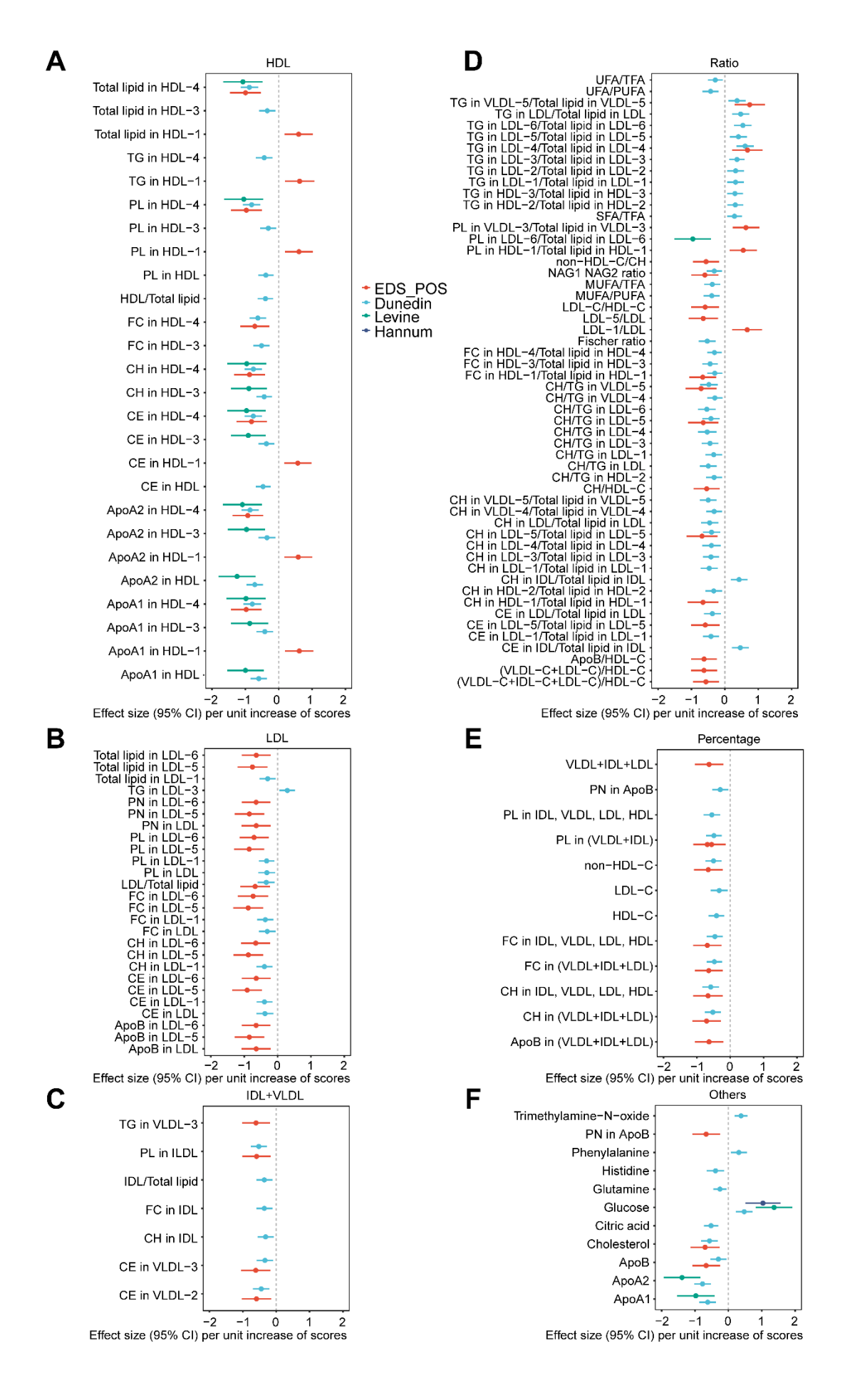
Given the significant influence of epigenetic mechanisms on lipid metabolism (Gomez-Alonso et al. 2021) and the observation that calorie restriction can modulate both epigenetic drift and metabolic pathways (Hahn et al. 2017; Maegawa et al. 2017), we further explored the impact of our EDS on serum lipid metabolites. We analyzed data from 3,037 individuals in the NSPT cohort, for whom both metabolomic and methylation profiles were available. The metabolomic dataset included 351 NMR-detected lipoprotein subfractions, comprising 176 direct measurements and 175 derived values.

After adjusting for age, gender, BMI, and sampling location, EDS_POS was significantly associated with 65 lipid metabolites following FDR correction (Fig. 6A-F, Supplemental Table S6). These associations encompassed 13 high-density lipoprotein (HDL) metrics, 17 low-density lipoprotein (LDL) metrics, 1 intermediate-density lipoprotein (IDL) metric, and 3 very-low-density lipoprotein (VLDL) metrics. Among the negative associations, EDS_POS showed the strongest correlation with phospholipids in HDL-4 ($p = 4.1 \times 10^{-3}$ after FDR). Among the positive associations, EDS_POS was most significantly associated with triglycerides in VLDL-5 (V5TGp, $p = 2.3 \times 10^{-2}$ after FDR), consistent with

--

previous studies that reported reduced VLDL levels in long-lived and younger cohorts (Lv et al. 2015). In addition to lipid metabolites, we examined the association of EDS with 17 physical and blood biochemical indicators. After adjusting for age, EDS_POS was significantly associated 6 out of 17 indicators, i.e., BMI, HDL, triglycerides (TG), uric acid (UA), indirect bilirubin (IBIL), and creatinine (CREA) (FDR p < 0.05). EDS_NEG did not show any significant association in lipid or blood biochemical association analyses (p>0.05 after FDR). Notably, further adjusting for clock scores in these association analyses did not alter our findings except for those related to UA (Supplemental Fig. S7).

Extending the lipid and blood biochemical association analyses to other epigenetic scores, including Hannum, Horvath, Levine, and Dunedin (Fig. 6 A-F), we identified numerous significant associations after adjusting for age. The strongest was between the Dunedin score and ApoA2 in HDL-4 ($p = 1.25 \times 10^{-8}$). In terms of the number of associations, the Dunedin score exhibited the most extensive associations, with 97 metabolites and 13 blood biochemical indicators, followed by EDS_POS (65 and 6), Levine (16 and 3), Hannum (1 and 2), and Horvath (0 and 6). Notably, further adjusting for clock scores in these association analyses did not alter our findings (Supplemental Fig. S8). Although the metabolites and biochemical indicators are strongly intercorrelated, our results suggest that multiple epigenetic scores play complex roles in metabolic features related to lipid metabolism, kidney function, and liver function.



449

450

451

452

453

454

455

456

457

458

459

460

461

462

463

464

465

466

467

468

469

470

471

472

Figure 6. Associations of EDS POS with serum lipid metabolic profiles. Forest plots display effect sizes (with 95% confidence intervals) per unit increase of relevant scores on various lipid metrics. The significance threshold for associations shown is set at FDR p < 0.05. Four epigenetic indicators are presented: EDS POS (red), Dunedin (light blue), Levine (green), and Hannum (dark blue). A, Associations with HDL-related traits. B, Associations with LDL-related traits. C, Associations with IDLand VLDL-related traits. **D**, Associations with lipid ratio metrics. **E**, Associations with lipid percentage metrics. F, Associations with other small metabolites and apolipoproteins. Abbreviations used in the figure include: ApoA1, ApoA2, ApoB (Apolipoprotein A1, Apolipoprotein A2, Apolipoprotein B); CH (Cholesterol); CE (Cholesteryl Esters); FA (Fatty Acids); FC (Free Cholesterol); HDL (High-Density Lipoprotein); IDL (Intermediate-Density Lipoprotein); LDL (Low-Density Lipoprotein); PL (Phospholipids); PN (Particle Number); TG (Triglycerides); UFA/TFA (Unsaturated Fatty Acids / Total Fatty Acids ratio); VLDL (Very Low-Density Lipoprotein); Subclass numbers indicate size-based lipoprotein subfractions. A complete list of all metabolite abbreviations and their full names is provided in Supplemental Table S6. GWAS on EDS identify genetic factors We conducted separate genome-wide association studies (GWAS) for EDS POS and EDS NEG, analyzing 8.6 million SNPs from microarray data after imputation in 3,513 individuals. No evidence of population sub-stratification was observed, as indicated by the inflation factor ($\lambda < 1.03$). The SNP-based heritability was estimated to be moderate for both traits using GCTA (EDS POS VG/VP = 0.29, se = 0.07; EDS NEG VG/VP = 0.11, se = 0.07). The GWAS for EDS POS identified a single SNP (rs7868942) located within the ASTN2 gene on 9q33.1 showing a genome-wide significant association with EDS POS (lead SNP rs7868942, $\beta = 0.02$, p = 4.3×10^{-8} , Fig. 7A-C). The ancestral A allele of rs7868942 had a frequency of 0.95 in our sample, similar to the East Asian (EAS) population frequency of 0.94, much higher than other continental groups in the 1000 Genomes Project (AMR 0.69, AFR 0.75, EUR 0.60, SAS 0.75). ASTN2 regulates neuronal

migration and synaptic strength by trafficking and degrading surface proteins, and has been repeatedly implicated in autism, Alzheimer's, and other neuropsychiatric disorders(Glessner et al. 2009; Ito et al. 2023). During aging, the chromatin state of *ASTN2* becomes more promoter-like and active, with a reduction in H3K36me3 and an accumulation of H3K4me3 and H3K27ac (Fig. 7D). This result is consistent with the previously proposed aging model, where reduced H3K36me3 levels within gene bodies inhibit the recruitment of KDM5B and DNMT3B to these regions, resulting in the accumulation of H3K4me3 and reduced DNA methylation, which leads to increased transcriptional noise(McCauley et al. 2021).

The GWAS for EDS NEG identified 20 SNPs on 2p21 near the SOCS5 gene that showed genome-wide significant associations with EDS NEG (lead SNP rs76089707, $\beta = -0.02$, $p = 1.2 \times 10^{-8}$, Fig. 7E-G). The ancestral G allele of rs76089707 had a frequency of 0.53 in our sample, closely matching the EAS population frequency of 0.52 and remaining comparable to frequencies in other continental groups from the 1000 Genomes Project (AMR 0.47, AFR 0.61, EUR 0.65, SAS 0.56). SOCS5, a cytokine signaling suppressor, negatively regulates the JAK/STAT pathway and plays a key role in balancing immune response and virus persistence (Seki et al. 2002; Kedzierski et al. 2022). While aging, T cells often experience increased activation and proliferation, leading to functional exhaustion. This exhaustion is linked to sustained JAK/STAT pathway activation, where SOCS proteins play a crucial inhibitory role(Sharma et al. 2019). During aging, the chromatin state of SOCS5 becomes more active, with an accumulation of H3K4me3 and H3K27ac, yet without a decrease in H3K36me3 (Fig. 7H). In exhausted T cells, specific CpG sites may become epigenetically stable, contributing to the long-term repression or activation of certain genes. While these preliminary findings provide valuable insights, the modest effect sizes and the proximity of the results to the genome-wide significance threshold suggest a cautious interpretation. Further validation through replication studies and functional assays is essential to confirm and elucidate the roles of these genomic loci in epigenetic drift.

473

474

475

476

477

478

479

480

481

482

483

484

485

486

487

488

489

490

491

492

493

494

495

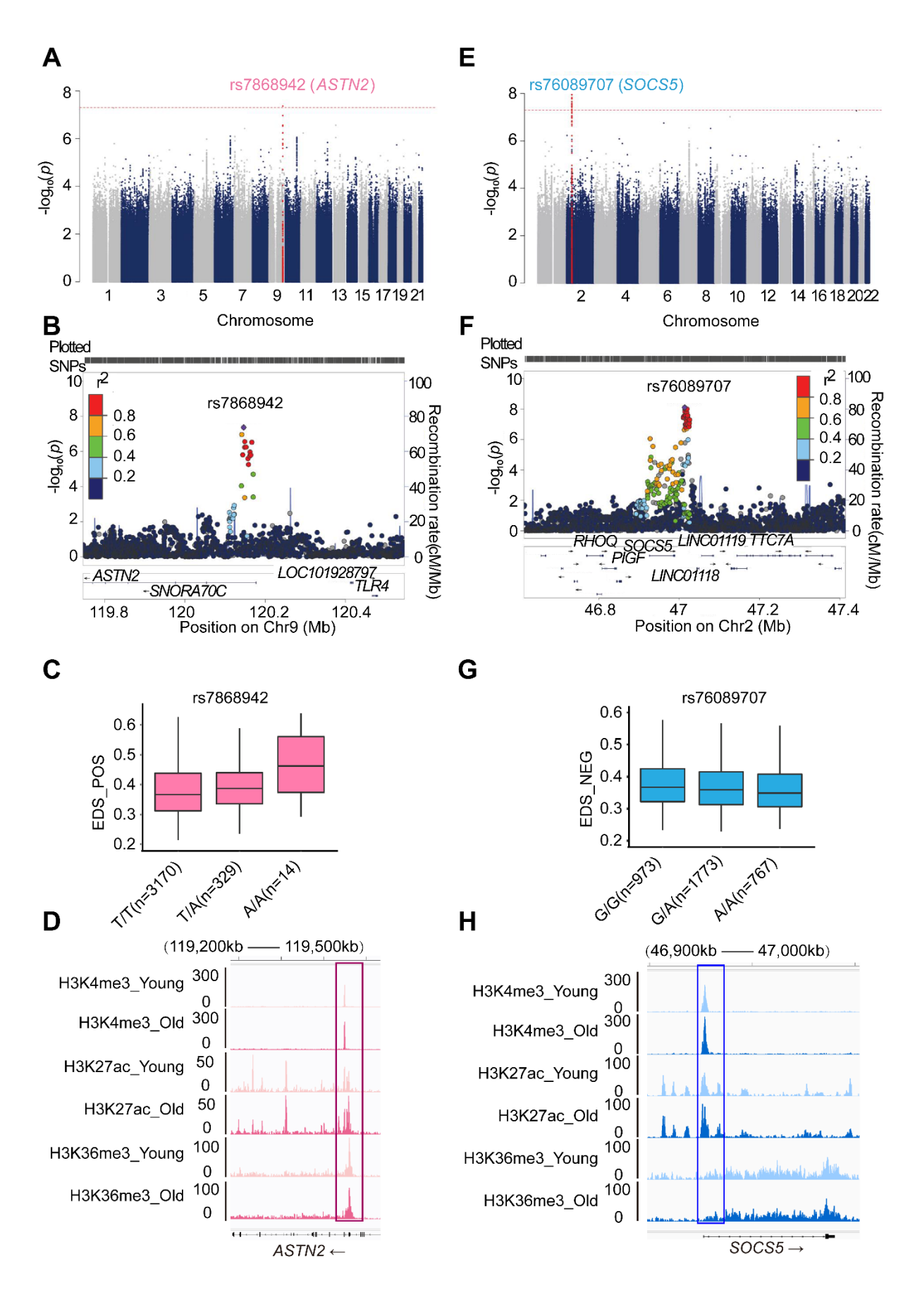


Figure 7. GWAS results for Epigenetic Drift Scores (EDS).

A, Manhattan plot showing SNP associations with EDS_POS. **B**–**C**, Locus zoom plot (B) and genotype-specific differences (C) for lead SNP rs7868942 near *ASTN2*. **D**, Aging is associated with a more active chromatin state at *ASTN2* (loss of H3K36me3; gain of H3K4me3, H3K27ac). **E**, Manhattan plot showing SNP associations with EDS_NEG. **F**–**G**, Locus zoom plot (F) and genotype-specific differences (G) for rs76089707 near *SOCS5*. **H**, *SOCS5* chromatin becomes more active with age in hMSCs, marked by increased H3K4me3 and H3K27ac enrichment (McCauley et al. 2021).

Discussion

499

500

501

502

503

504

505

506

507

508

509

510

511

512

513

514

515

516

517

518

519

520

521

522

523

In this study, we present the largest EWDS to date, conducted in a Chinese population and replicated in multiple Chinese and European cohorts. We systematically benchmarked statistical approaches for detecting heteroscedasticity in DNA methylation data and identified White's test as the most robust method. Applying this approach, we identified and functionally annotated over 50,000 significant drift-CpGs, which segregated into positive and negative drift categories with distinct genomic enrichments, suggesting divergent underlying biological mechanisms. Integration with single-cell RNA sequencing revealed that drift-associated CpGs exert direction-specific transcriptional effects and display marked cell-type specificity. We further developed and validated composite EDS POS and EDS NEG to quantify individual-level drift, both of which showed strong correlations with chronological age. Notably, positive EDS was significantly associated with lipidomic profiles, as well as metabolic and clinical health indicators. Importantly, the population-level drift-CpGs and EDS signatures were also validated longitudinally at the individual level. Finally, genome-wide association analyses identified genetic loci, including ASTN2 and SOCS5, associated with positive and negative drift variation, respectively, underscoring a heritable component. Together, these findings offer key conceptual and methodological advances in mapping epigenetic drift and underscore its significance in aging biology and age-related disease susceptibility.

525

526

527

528

529

530

531

532

533

534

535

536

537

538

539

540

541

542

543

544

545

546

547

548

549

Our findings reveal that both positive and negative epigenetic drift are associated with aging, yet they likely represent distinct biological processes with divergent regulatory consequences. Positive drift, characterized by increased methylation variance with age, is more prevalent genome-wide and typically occurs in CpG island (CGI)-rich regions (Slieker et al. 2016). It exhibits minimal dependence on immune cell composition, suggesting a population-wide, stochastic process. Functionally, positive drift is associated with increased gene expression variability, i.e., transcriptional noise, particularly in genes linked to neurological and metabolic pathways. These changes may reflect compensatory or stressinduced transcriptional activation and contribute to systemic dysregulation observed in aging, including altered lipid metabolism and blood biomarkers. Despite having a smaller effect size than traditional epigenetic clocks, we show that a subset of ~200 key drift-CpGs can effectively summarize genome-wide stochastic methylation variability. These results support the notion that positive drift captures nonprogrammatic, nonlinear aspects of aging, potentially serving as a mechanistic substrate for the emergence of epigenetic clocks themselves through cumulative stochastic changes. In contrast, negative drift, though less common, is enriched in enhancer regions and exhibits strong CD4⁺ T cell-specific patterns. It is associated with reduced transcriptional noise in aged individuals and appears to reflect immune-specific regulatory stabilization, rather than general epigenomic entropy. Mechanistically, negative drift is enriched for binding sites of transcription factors such as AHR and may participate in fine-tuning immune gene regulation during aging (Salminen 2022). This is consistent with prior observations of age-associated T cell depletion, immune remodeling, and skewing of CD4⁺ T cells toward extreme regulatory and effector phenotypes (Dorshkind et al. 2009; Elyahu et al. 2019). Specifically, aging might reduce CD4+ T cell numbers and reshape their composition, potentially driving the emergence of distinct DNA methylation patterns linked to negative drift. Thus, while positive drift may reflect stochastic cellular deterioration, negative drift may represent an adaptive or programmed component of immune aging. These distinct patterns suggest that epigenetic drift is not a monolithic process, but rather a bifurcated aging mechanism—stochastic (positive) versus programmed (negative) with far-reaching implications for identifying aging biomarkers and designing targeted interventions.

While some previous studies have proposed that epigenetic drift may contribute to the generation of epigenetic clocks (Meyer and Schumacher 2024), our findings suggest that epigenetic drift appears to represent a distinct dimension of epigenetic aging, primarily reflecting the accumulation of stochastic, non-programmatic changes over time. In contrast, epigenetic clocks are typically derived from CpGs whose methylation levels change in a coordinated and directional manner with age, likely reflecting functional, environmentally responsive, or developmentally regulated processes. This distinction is supported by the only moderate correlations we observed between the EDS and established epigenetic age estimators(Hannum et al. 2013; Horvath 2013; Levine et al. 2018; Belsky et al. 2020). Unlike clocks, which are trained to predict chronological or biological age, the EDS captures genome-wide epigenomic instability irrespective of directionality. We therefore interpret positive drift as a signature of cumulative random damage or loss of epigenetic maintenance fidelity, rather than a direct mechanistic contributor to clock formation.

Our study demonstrates that drift-CpGs and the EDS capture cumulative, age-related epigenetic variability at the individual level. Validated examples—such as positive drift at FBXO2 and LINC02716 and negative drift at FOXK1 and TCF12—highlight their relevance to transcriptional regulation and disease. Inter-individual differences in EDS further support its utility in quantifying genome-wide drift and predicting aging-related traits. Notably, we found significant associations between EDS and lipid metabolism, particularly with subclasses of LDL and HDL, underscoring a potential regulatory link.

These results align with prior studies on DNA methylation and lipoproteins (Gomez-Alonso et al. 2021) and suggest the need for further functional investigation into the causal role of epigenetic drift in lipid regulation. Our study suggests potential sex-specific differences in epigenetic aging, with females exhibiting a slower accumulation of positive epigenetic drift compared to males. This observation may reflect greater epigenomic stability in females against age-associated stochastic changes, potentially influenced by hormonal or chromatin-related factors. While these findings may offer a partial explanation

for the observed female longevity advantage, they also highlight the importance of considering sex as a biological variable in the development of aging biomarkers and potential interventions.

Our analysis focused on identifying drift-CpGs using population-level, cross-sectional DNA methylation array data. In contrast, some other studies have proposed metrics such as Shannon entropy or the proportion of intermediately methylated sites to quantify methylation heterogeneity within individual samples (Scherer et al. 2020). These entropy-based measures typically require deep bisulfite sequencing (e.g., WGBS) to resolve single-molecule differences. Although we also calculated individual-level entropy from array data, our primary objective was to model changes in methylation variance with age across the population, enabling the identification of drift-CpGs that reflect systemic epigenetic variability rather than within-sample noise. This focus is partly driven by data availability: while WGBS offers near-complete CpG coverage and can assess cell-intrinsic variability, the EPIC array surveys a fixed subset of CpGs and reflects averaged methylation signals across heterogeneous cell populations. Importantly, we validated the drift-CpGs identified at the population level using independent longitudinal datasets, supporting their temporal robustness. Furthermore, the EDS derived from drift-CpGs showed a strong correlation with entropy-based measures, suggesting that these two approaches, though methodologically distinct, converge on capturing common aspects of epigenetic aging.

Nevertheless, we acknowledge several limitations. First, our study lacks multi-tissue or large-scale longitudinal data spanning broader age ranges, which are necessary to evaluate drift dynamics across developmental and aging trajectories. Second, our analysis is based on array-derived methylation data rather than whole-genome bisulfite sequencing, potentially limiting the detection of drift in non-CpG sites and distal regulatory elements. Third, we did not integrate matched transcriptomic or additional epigenomic layers, which constrains our ability to systematically assess the downstream regulatory consequences of drift. Future studies employing multi-omic, single-cell, and longitudinal designs across diverse tissues and larger cohorts will be critical to further refine and validate our model of epigenetic drift in human aging.

Methods

Study Cohorts, DNA Methylation, Serum Metabolomics, SNP Microarray and Phenotyping

Detailed descriptions of the NSPT, CAS, and Changfeng cohorts are provided in the Supplemental Methods. In brief, all cohorts consisted of Chinese individuals, and genome-wide DNA methylation was measured using the Illumina Infinium MethylationEPIC BeadChip. Written informed consent was obtained from all participants, and each study was approved by the respective institutional review board.

Genome-wide DNA methylation in all three cohorts was profiled using Illumina MethylationEPIC BeadChips. DNA extraction and bisulfite conversion followed published protocols (Xia et al. 2023; Peng et al. 2024). Raw .idat files were processed using minfi (NSPT) or CHAMP (CAS and Changfeng) without background correction. Quality control excluded samples with unclear gender and probes with SNPs, sex chromosome location, or high missingness. Missing values were imputed (impute.knn), Type-2 bias corrected (BMIQ), and batch effects adjusted (ComBat on M-values).

The NSPT cohort included detailed phenotypic data (e.g., height, weight, blood pressure) and 13 blood biochemical traits. Serum metabolomics on a subset was performed using a 600 MHz NMR platform (Bruker), analyzed with B.I.LISA™ and B.I.Quant-PS™ software (Wu et al. 2021). Genotyping was conducted using the Illumina Global Screening Array, followed by standard QC in PLINK and imputation with 1000 Genomes (SHAPEIT3 and IMPUTE2). After QC, 8,603,582 SNPs remained for analysis.

Statistical Analysis

White method for detecting epigenetic drift-CpGs

To identify epigenetic drift-CpGs, defined as CpG sites exhibiting age-related heteroscedasticity, we employed an improved two-step regression method based on White's heteroscedasticity test (White, 1980).

In the first step, we constructed a linear regression model (equation 1) using beta values of each CpG and age, calculating the squared residuals from the least squares regression while also correcting for potential confounding factors such as gender, BMI, and cell composition that may affect DNA methylation levels. Cell type proportions were estimated using the EpiDISH algorithm(Zheng et al. 2018).

$$\widehat{\beta}_i = \alpha_{1i} y + \alpha_{0i} + c$$
, (equation 1)

where α_{1i} and α_{0i} denote the estimated effect and bias of the ith CpG site, respectively. $y=(y_1, y_2, ..., y_n)$, $c=(c_1, c_2, ..., c_n)$, and $\hat{\beta}_i=(\hat{\beta}_{1i}, \hat{\beta}_{2i}, ..., \hat{\beta}_{ni})$ represent the age, covariates (gender, BMI, and cell composition), and estimated beta values of the ith CpG site for all samples, respectively, with n denoting the sample size. The deviation $d_i=(\beta_i-\widehat{\beta}_i)^2$ between the true beta value β_i and the estimated value $\widehat{\beta}_i$ reflects the degree of epigenetic drift at CpG site i under a given age.

In the second step, we regressed d_i on age using the following equation 2.

635
$$d_i = \gamma_{1i} y + \gamma_{2i} y^2 + \gamma_{0i}$$
, (equation 2)

where γ_{1i} , γ_{2i} and γ_{0i} denote the estimated age effect, age square effect and bias of the ith CpG site. To assess whether equation 2 significantly differs from the null model with no variables, we performed a hypothesis test on the model in equation (2) compared with model without age effect using a χ 2-statistic, and obtained the corresponding p-value.

Simulation benchmarking for heteroscedasticity testing of drift-CpGs

To evaluate the performance of existing heteroscedasticity testing methods in detecting epigenetic drift-CpGs, we conducted a comprehensive simulation study. We generated four distinct types of synthetic DNA methylation datasets: (1) a baseline dataset with no heteroscedasticity or outliers (to assess Type I error), (2) a dataset with outliers but no heteroscedasticity (to evaluate robustness to outliers), (3) a dataset exhibiting linear age-related heteroscedasticity, and (4) a dataset demonstrating non-linear age-related heteroscedasticity.

We then compared the Type I error and statistical power of four methods: Liu et al. (Method A, Double Generalized Linear Model using dglm R package), Bergstedt et al. (Method B, Heteroscedastic Likelihood Ratio Test using gamlss R package), Slieker et al. (Method C, Breusch-Pagan test), and our improved White method (Method D). Performance was evaluated based on false positive rates for Dataset 1, impact of outliers in Dataset 2, and statistical power for linear (Dataset 3) and nonlinear (Dataset 4) drift-CpGs. Detailed simulation parameters and method implementations are provided in Supplemental Methods.

Epigenome-Wide Drift Study (EWDS)

Prior to epigenome-wide drift analysis, we removed 342,815 CpGs from a total of 811,876 CpGs in the discovery NSPT dataset, including 284,128 DNA methylation CpGs, i.e., those significantly affected by mQTLs in Chinese populations (Peng et al. 2024), 57,691 CpGs with no variation (variance< 1×10^{-5}), and 996 CpGs failing the Multimodal distribution test (R-diptest, $p<1\times10^{-4}$), resulting in a total of 469,061 CpGs. Then we conducted epigenome-wide drift identification using the White method on these 469,061 CpGs and further investigated and compared the performance of the other three methods. P value smaller than 1×10^{-7} (Bonferroni p<0.05) were considered as epigenome-wide significant. Significant drift-CpGs were categorized into positive drift (age-increasing inter-individual variability) and negative drift (age-decreasing variability). Beyond identifying drift-CpGs, our analysis comprehensively characterized their properties and regulation through exploring correlations between DNA methylation variation and initial/terminal levels (details in Supplemental Methods).

Epigenome-wide association study (EWAS) for chronological age

To identify the age-associated CpGs, termed here as clock-CpGs, we used a linear model to perform epigenome wide association analysis based on 469,061 CpGs in the NSPT cohort with the same starting

amount as EWDS. P value smaller than 1×10^{-7} (Bonferroni p < 0.05) were considered as epigenome-wide significant. Covariates included gender, BMI, cell composition, experiment batch, the first 5 genetic principal components and the first 5 epigenetic principal components. Genomic principal components (genomic PCs) were calculated using PLINK 1.9 based on all genome-wide SNPs. For methylation principal components (methylation PCs), we applied the prcomp function in R to the β values of 810,000 CpG sites across the genome.

Cell-type-specific and Single-cell RNA-seq Integration

To assess cell-type-specific contributions to methylation drift, we adapted the CellDMC framework (Zheng et al. 2018), modeling the interaction between age and estimated cell-type proportion (estimated using EpiDISH) (Teschendorff and Zheng 2017), for significant drift-CpGs. For each CpG, age-dependent methylation drift specificity across cell types was assessed, with Bonferroni-adjusted p-values < 0.05 considered significant. To elucidate the contribution of age-related methylation drift to interindividual immune variation, we integrated population-scale epigenetic drift profiles with single-cell transcriptomic data from peripheral blood mononuclear cells (PBMCs) in the OneK1K cohort(Yazar et al. 2022). We compared transcriptional dynamics between individuals at the extremes of the age spectrum. The BASiCS algorithm (Vallejos et al. 2015) was used to estimate age-associated changes in both transcriptional levels and noise, stratified by methylation drift direction.

Biological Annotations

CpGs were mapped to the hg19 build for genomic annotations (e.g., Enhancer, TSS1500, TSS200, UTR5, 1stExon, ExonBnd, Body, UTR3, Promoter) and CpG island annotations (N_Shelf, N_Shore, Island, S_Shore, S_Shelf). Relative enrichment analysis of chromosome states and gene regions was conducted separately for positive/negative drift and clock CpGs. Significance was assessed using a hypergeometric test (p < 0.05). The formula for odds ratio calculation and detailed annotation categories are in Supplemental Methods. Transcription Factor Binding Site (TFBS) Enrichment Analysis on drift-CpGs

was performed using the TFmotifView web tool (https://bardet.u-strasbg.fr/tfmotifview/), extracting 10 bp sequence windows centered on each CpG site. Statistical significance was assessed using Bonferroni correction (adjusted p < 0.05). We drift-CpGs for enrichment of gene ontologies and KEGG pathways using the gometh function using R package 'missmethyl' (v1.28.0). Using the online analysis platform EWAS atlas, we performed phenotype enrichment analysis on successfully validated drift-CpGs. To explore the distinct biological functions associated with positive and negative drift, we performed enrichment analyses separately for the sets of positive drift-CpGs and negative drift-CpGs, applying a significance threshold of 0.05 after FDR adjustment.

Replication Analysis

Drift-CpGs significant in the NSPT discovery analysis (p<1×10⁻⁷) were followed up with a replication analysis in the CAS cohort using the White method. Further validation was performed in the GSE40279 dataset (a mixed Caucasian and Hispanic population assessed with a 450K beadchip) (Hannum et al. 2013). In the longitudinal Changfeng population, CpG drift values between two time points were calculated and analyzed using paired t-tests. The stability of drift was also investigated in the GSE61496 twin cohort (Tan et al. 2014) using linear regression on absolute age differences and twin pair values.

Construction of Epigenetic Drift Score (EDS)

To quantify an individual's epigenetic drift burden, we developed the Epigenetic Drift Score (EDS). This score aggregates individual-level methylation variability at robustly selected CpGs, reflecting an individual's overall drift status. First, we selected highly robust drift-CpGs, defined as those significantly associated with age-related variability in the NSPT discovery cohort and consistently replicated in both CAS and Hannum cohorts. To ensure independence, CpGs within 500-kb proximity of a more significant CpG were removed. Specific filtering criteria and the final number of independent CpGs are detailed in Supplemental Methods.

For each individual i and selected drift site j, we computed the site-specific drift magnitude (d_{ij}) as the squared deviation of methylation level from the mean, scaled by the site's standard deviation: $d_{ij} = \beta_{ij} - \bar{\beta_j}^2/SD_j$, where d_{ij} denotes the drift magnitude for individual i at site j, β_{ij} is the methylation level for individual i at site j, $\bar{\beta_j}$ is the mean methylation level at site j, and SD_j is the standard deviation of methylation at site j. To derive weights for aggregation, a non-negative least squares regression between each site's drift score d_{ij} and the age of the individual y_i was then performed, $y_i = \alpha + \gamma_j d_{ij}$, where α is the intercept term and γ_j is the regression coefficient reflecting the correlation between drift score and age. The overall positive epigenetic drift score EDS_POS_i for individual i was then calculated by summing across selected sites (K), weighted by their respective non-negative regression coefficients (γ_j) : $EDS_POS_i = \sum_{j=1}^K \gamma_j d_{ij}$

These weighting factors, derived from the NSPT and Hannum cohorts, serve as a standard reference. Scores were subsequently range-normalized to a 0-1 scale using reference populations to project minimum and maximum possible scores. The negative epigenetic drift score (EDS_NEG) was constructed following a similar approach. This involved using significant negative drift-CpGs from the NSPT cohort, applying a non-negative least squares regression model to identify contributing sites, and then range-standardizing the scores to a 0-1 scale (details on site selection and final number of sites in Supplemental Methods). As a validation, we also implemented an entropy-based approach (Scherer et al. 2020) to measure individual-level DNA methylation variability. Genome-wide Shannon entropy was computed for positive and negative drift-CpGs, and its concordance with EDS values was assessed (details and formula in Supplemental Methods).

Association of EDS with age, metabolome, and genetic variants

We evaluated correlations between EDS and chronological age in the NSPT and CAS cohorts and assessed EDS distributions across gender groups. In the NSPT cohort, we used linear regression to test

associations between EDS and NMR-derived lipoprotein subfractions and small metabolites, adjusting for covariates (see Supplemental Methods). Significance was determined using FDR-adjusted p < 0.05. GWAS of EDS in NSPT was conducted using linear regression models in PLINK, adjusting for relevant covariates. EDS heritability was estimated using GCTA. Age-associated chromatin state changes at key loci were visualized using the Integrative Genomics Viewer (IGV) with hMSC ChIP-seq data from GSE156409 (McCauley et al. 2021).

Published Software and Resources

Publicly available software and R packages utilized in this study include: R (V4.4.0)(R Core Team 2024), ggplot2, diptest, missMethyl, poolr, corrplot, forestplot, SHAPEIT3, IMPUTE2, PLINK2.0, GCTA, and IGV (URLs in Supplemental Methods).

Ethics declarations

The NSPT study was approved by the Ethics Committee of Human Genetic Resources of the School of Life Sciences, Fudan University, Shanghai (14117). CAS study was approved by the Institutional Review Board of Beijing Institute of Genomics and Zhongguancun Hospital (2020H020, 2021H001 and 20201229). Shanghai Changfeng Study was approved by the Research Ethics Committee of Zhongshan Hospital, Fudan University (No. 2008-119 and B2013-132). All participants provided written informed consent to participate in the study and to have their information obtained from treating physicians.

Data access

757

768

769

770

771

772

773

774

775

776

777

778

779

780

781

782

783

- All DNA methylation data generated in this study have been deposited in publicly accessible databases.
- 759 The CAS cohort data are available at OMIX (https://ngdc.cncb.ac.cn/omix/) under accession code
- 760 OMIX004333. The NSPT and Changfeng cohort data are available at the National Omics Data
- 761 Encyclopedia (NODE, https://www.biosino.org/node) under accession numbers OEZ00008120 (NSPT
- 762 cohort: file name: methy 3523.rdata) and OEP00004768 (Changfeng cohort). Individual-level genotype
- data can also be requested through NODE under accession number OEZ00008120. Data usage shall be in
- compliance with the 2023 Implementation Rules for the Management Regulations of Human Genetic
- Resources issued by China's Ministry of Science and Technology (MOST). The source codes used in this
- study to identify and quantify epigenetic drift, and to generate corresponding graphs, are available at
- 767 GitHub (https://github.com/Fun-Gene/EpigeneticDriftScore) and as Supplemental Code.

Competing interest statement

The authors declare no competing interests.

Acknowledgements

The authors are grateful for the dedication, commitment and contribution of the study participants, the general practitioners, pharmacists, Human Phenome Data Center of Fudan University, and the staff from the NSPT, CAS, and Chengfeng Study. We thank Mr. Yuan Cheng for valuable discussions on statistical aspects of the heteroscedasticity test. FL was supported by the Strategic Priority Research Program of Chinese Academy of Sciences (Grant No. XDB38010400, XDC010000000), Shanghai Municipal Science and Technology Major Project (Grant No. 2017SHZDZX01), National Natural Science Foundation of China (NSFC) (81930056), Science and Technology Service Network Initiative of Chinese Academy of Sciences (KFJ-STS-QYZD-2021-08-001, KFJ-STS-ZDTP-079), and Naif Arab University for Security Sciences (NAUSS-23-R17, NAUSS-23-R18, NAUSS-23-R19). SW was supported by the National Natural Science Foundation of China (NSFC) (Grant No. 92249302), the National Natural Science Foundation of China (NSFC) (Grant No. 92249302), the National Natural Science Foundation of China (NSFC) (Grant No. 92325013), the CAS Project for Young Scientists in Basic Research, Grant No. YSBR-077, the Strategic Priority Research Program of the Chinese Academy of Sciences (Grant No. XDB38020400 to SW), Shanghai Science and Technology Commission Excellent

- 784 Academic Leaders Program (22XD1424700) and was supported by the Human Phenome Data Center of
- Fudan University. XG was supported by Shanghai Municipal Science and Technology Major Project 785
- (Grant No. 2017SHZDZX01). MX was supported by National Natural Science Foundation of China 786
- (Grant No. 32371333) and Program of Shanghai Academic Research leader (Grant No. 23XD1423300). 787
- 788 WL was supported by National Natural Science Foundation of China (NSFC) (Grant No. 32200472) and
- 789 China Postdoctoral Science Foundation (Grant No. 2021M693274 and BX2021336).
- 790 Author contributions:
- 791 Xiu Fan and Fan Liu conceived the study. Xiu Fan and Qili Qian developed mathematical formulations,
- performed data analyses, developed computer pipeline, visualized, and interpreted results. Tianzi Liu, 792
- 793 Wenran Li and Huandong Lin contributed to data collection. Changqing Zeng, Peilin Jia, Huandong Lin,
- 794 Xin Gao, Mingfeng Xia, Li Jin, Sijia Wang, Fan Liu provided the data resource and obtained funding.
- 795 Xiu Fan, Qili Qian and Fan Liu drafted the initial manuscript. All authors approved the submission of the
- 796 final version of the article for publication.
- 797 References

803

804

807

808

809

- Bazzocco S, Dopeso H, Martínez-Barriocanal Á, Anguita E, Nieto R, Li J, García-Vidal E, Maggio V, 798 Rodrigues P. de Marcondes PG et al. 2021. Identification of ZBTB18 as a novel colorectal tumor 799 800 suppressor gene through genome-wide promoter hypermethylation analysis. Clin Epigenetics 13: 801 88.
 - Belsky DW, Caspi A, Arseneault L, Baccarelli A, Corcoran DL, Gao X, Hannon E, Harrington HL, Rasmussen LJ, Houts R et al. 2020. Quantification of the pace of biological aging in humans through a blood test, the DunedinPoAm DNA methylation algorithm. Elife 9: e54870.
- Bergstedt J, Azzou SAK, Tsuo K, Jaquaniello A, Urrutia A, Rotival M, Lin DTS, MacIsaac JL, Kobor 805 806 MS, Albert ML et al. 2022. The immune factors driving DNA methylation variation in human blood. Nat Commun 13: 5895.
 - Ciceri G, Baggiolini A, Cho HS, Kshirsagar M, Benito-Kwiecinski S, Walsh RM, Aromolaran KA, Gonzalez-Hernandez AJ, Munguba H, Koo SY et al. 2024. An epigenetic barrier sets the timing of human neuronal maturation. Nature 626: 881-890.
- Dorshkind K, Montecino-Rodriguez E, Signer RA. 2009. The ageing immune system: is it ever too old to 811 812 become young again? Nat Rev Immunol 9: 57-62.
- 813 Elyahu Y, Hekselman I, Eizenberg-Magar I, Berner O, Strominger I, Schiller M, Mittal K, Nemirovsky 814 A, Eremenko E, Vital A et al. 2019. Aging promotes reorganization of the CD4 T cell landscape toward extreme regulatory and effector phenotypes. Sci Adv 5: eaaw8330. 815
- 816 Feinberg AP, Levchenko A. 2023. Epigenetics as a mediator of plasticity in cancer. Science 379: 817 eaaw3835.

- Fraga MF, Ballestar E, Paz MF, Ropero S, Setien F, Ballestar ML, Heine-Suñer D, Cigudosa JC, Urioste M, Benitez J et al. 2005. Epigenetic differences arise during the lifetime of monozygotic twins.

 Proc Natl Acad Sci U S A 102: 10604-10609.
- Fujinuma S, Nakatsumi H, Shimizu H, Sugiyama S, Harada A, Goya T, Tanaka M, Kohjima M,
 Takahashi M, Izumi Y et al. 2023. FOXK1 promotes nonalcoholic fatty liver disease by
 mediating mTORC1-dependent inhibition of hepatic fatty acid oxidation. *Cell Rep* **42**: 112530.

- Glessner JT, Wang K, Cai G, Korvatska O, Kim CE, Wood S, Zhang H, Estes A, Brune CW, Bradfield JP et al. 2009. Autism genome-wide copy number variation reveals ubiquitin and neuronal genes. *Nature* **459**: 569-573.
- Gomez-Alonso MDC, Kretschmer A, Wilson R, Pfeiffer L, Karhunen V, Seppala I, Zhang W, Mittelstrass K, Wahl S, Matias-Garcia PR et al. 2021. DNA methylation and lipid metabolism: an EWAS of 226 metabolic measures. *Clinical epigenetics* **13**: 7.
- Hahn O, Grönke S, Stubbs TM, Ficz G, Hendrich O, Krueger F, Andrews S, Zhang Q, Wakelam MJ, Beyer A et al. 2017. Dietary restriction protects from age-associated DNA methylation and induces epigenetic reprogramming of lipid metabolism. *Genome Biology* **18**.
- Hannum G, Guinney J, Zhao L, Zhang L, Hughes G, Sadda S, Klotzle B, Bibikova M, Fan JB, Gao Y et al. 2013. Genome-wide methylation profiles reveal quantitative views of human aging rates. *Mol Cell* **49**: 359-367.
- Horvath S. 2013. DNA methylation age of human tissues and cell types. *Genome Biol* 14: R115.
- Horvath S, Raj K. 2018. DNA methylation-based biomarkers and the epigenetic clock theory of ageing. *Nat Rev Genet* **19**: 371-384.
- Ito T, Yoshida M, Aida T, Kushima I, Hiramatsu Y, Ono M, Yoshimi A, Tanaka K, Ozaki N, Noda Y. 2023. Astrotactin 2 (ASTN2) regulates emotional and cognitive functions by affecting neuronal morphogenesis and monoaminergic systems. *J Neurochem* **165**: 211-229.
- Kedzierski L, Tan AEQ, Foo IJH, Nicholson SE, Fazakerley JK. 2022. Suppressor of Cytokine Signalling 5 (SOCS5) Modulates Inflammatory Responses during Alphavirus Infection. *Viruses* 14.
- Landau DA, Clement K, Ziller MJ, Boyle P, Fan J, Gu H, Stevenson K, Sougnez C, Wang L, Li S et al. 2014. Locally disordered methylation forms the basis of intratumor methylome variation in chronic lymphocytic leukemia. *Cancer Cell* 26: 813-825.
- Levine ME, Lu AT, Quach A, Chen BH, Assimes TL, Bandinelli S, Hou L, Baccarelli AA, Stewart JD, Li Y et al. 2018. An epigenetic biomarker of aging for lifespan and healthspan. *Aging (Albany NY)* **10**: 573-591.
- Li Y, Tollefsbol TO. 2016. Age-related epigenetic drift and phenotypic plasticity loss: implications in prevention of age-related human diseases. *Epigenomics* **8**: 1637 1651.
- Liu EA, Schultz ML, Mochida C, Chung C, Paulson HL, Lieberman AP. 2020. Fbxo2 mediates clearance of damaged lysosomes and modifies neurodegeneration in the Niemann-Pick C brain. *JCI Insight* 5.
- Liu Y, Sinke L, Jonkman TH, Slieker RC, van Zwet EW, Daxinger L, Heijmans BT. 2023. The inactive X chromosome accumulates widespread epigenetic variability with age. *Clin Epigenetics* **15**: 135.
- López-Otín C, Blasco MA, Partridge L, Serrano M, Kroemer G. 2023. Hallmarks of aging: An expanding universe. *Cell* **186**: 243-278.
- Lv Y-B, Yin Z-X, Chei C-L, Qian H-Z, Kraus VB, Zhang J, Brasher MS, Shi X-M, Matchar DB, Zeng Y. 2015. Low-density lipoprotein cholesterol was inversely associated with 3-year all-cause mortality among Chinese oldest old: Data from the Chinese Longitudinal Healthy Longevity Survey. *Atherosclerosis* 239: 137-142.
- Maegawa S, Lu Y, Tahara T, Lee JT, Madzo J, Liang S, Jelinek J, Colman RJ, Issa JJ. 2017. Caloric restriction delays age-related methylation drift. *Nat Commun* **8**: 539.
- McCauley BS, Sun L, Yu R, Lee M, Liu H, Leeman DS, Huang Y, Webb AE, Dang W. 2021. Altered Chromatin States Drive Cryptic Transcription in Aging Mammalian Stem Cells. *Nat Aging* 1: 684-697.

- Meyer DH, Schumacher B. 2024. Aging clocks based on accumulating stochastic variation. *Nat Aging* **4**: 871-885.
- Peng Q, Liu X, Li W, Jing H, Li J, Gao X, Luo Q, Breeze CE, Pan S, Zheng Q et al. 2024. Analysis of blood methylation quantitative trait loci in East Asians reveals ancestry-specific impacts on complex traits. *Nature Genetics* **56**: 846-860.

- Planterose Jimenez B, Liu F, Caliebe A, Montiel Gonzalez D, Bell JT, Kayser M, Vidaki A. 2021. Equivalent DNA methylation variation between monozygotic co-twins and unrelated individuals reveals universal epigenetic inter-individual dissimilarity. *Genome Biol* 22: 18.
 - R Core Team. 2024. R: A Language and Environment for Statistical Computing. R Foundation for Statistical Computing.
 - Salminen A. 2022. Aryl hydrocarbon receptor (AhR) reveals evidence of antagonistic pleiotropy in the regulation of the aging process. *Cellular and Molecular Life Sciences: CMLS* **79**.
 - Scherer M, Nebel A, Franke A, Walter J, Lengauer T, Bock C, Müller F, List M. 2020. Quantitative comparison of within-sample heterogeneity scores for DNA methylation data. *Nucleic Acids Research* **48**: e46-e46.
 - Seale K, Horvath S, Teschendorff A, Eynon N, Voisin S. 2022. Making sense of the ageing methylome. *Nat Rev Genet* **23**: 585-605.
 - Seki Y, Hayashi K, Matsumoto A, Seki N, Tsukada J, Ransom J, Naka T, Kishimoto T, Yoshimura A, Kubo M. 2002. Expression of the suppressor of cytokine signaling-5 (SOCS5) negatively regulates IL-4-dependent STAT6 activation and Th2 differentiation. *Proc Natl Acad Sci U S A* **99**: 13003-13008.
 - Shah S, McRae AF, Marioni RE, Harris SE, Gibson J, Henders AK, Redmond P, Cox SR, Pattie A, Corley J et al. 2014. Genetic and environmental exposures constrain epigenetic drift over the human life course. *Genome Research* **24**: 1725 1733.
 - Sharma ND, Nickl CK, Kang H, Ornatowski W, Brown R, Ness SA, Loh ML, Mullighan CG, Winter SS, Hunger SP et al. 2019. Epigenetic silencing of SOCS5 potentiates JAK-STAT signaling and progression of T-cell acute lymphoblastic leukemia. *Cancer Sci* **110**: 1931-1946.
 - Slieker RC, van Iterson M, Luijk R, Beekman M, Zhernakova DV, Moed MH, Mei H, van Galen M, Deelen P, Bonder MJ et al. 2016. Age-related accrual of methylomic variability is linked to fundamental ageing mechanisms. *Genome Biol* 17: 191.
 - Tan Q, Frost M, Heijmans BT, von Bornemann Hjelmborg J, Tobi EW, Christensen K, Christiansen L. 2014. Epigenetic signature of birth weight discordance in adult twins. *BMC Genomics* **15**: 1062.
 - Tan Q, Heijmans BT, Hjelmborg JV, Soerensen M, Christensen K, Christiansen L. 2016. Epigenetic drift in the aging genome: a ten-year follow-up in an elderly twin cohort. *Int J Epidemiol* **45**: 1146-1158.
 - Teschendorff AE, Zheng SC. 2017. Cell-type deconvolution in epigenome-wide association studies: a review and recommendations. *Epigenomics* **9**: 757-768.
 - Vallejos CA, Marioni JC, Richardson S. 2015. BASiCS: Bayesian Analysis of Single-Cell Sequencing Data. *PLoS Comput Biol* 11: e1004333.
 - Wang R, Bhatt AB, Minden-Birkenmaier BA, Travis OK, Tiwari S, Jia H, Rosikiewicz W, Martinot O, Childs E, Loesch R et al. 2023. ZBTB18 restricts chromatin accessibility and prevents transcriptional adaptations that drive metastasis. *Sci Adv* 9: eabq3951.
 - Wang Y, Pedersen NL, Hägg S. 2018. Implementing a method for studying longitudinal DNA methylation variability in association with age. *Epigenetics* **13**: 866-874.
- 912 White H. 1980. A Heteroskedasticity-Consistent Covariance Matrix Estimator and a Direct Test for Heteroskedasticity. *Econometrica* **48**: 817-838.
- Wu Q, Huang Q-x, Zeng H-l, Ma S, Lin H-d, Xia M-f, Tang H-r, Gao X. 2021. Prediction of Metabolic
 Disorders Using NMR-Based Metabolomics: The Shanghai Changfeng Study. *Phenomics* 1: 186-198.

- Xia M, Li W, Lin H, Zeng H, Ma S, Wu Q, Ma H, Li X, Pan B, Gao J et al. 2023. DNA methylation age
 acceleration contributes to the development and prediction of non-alcoholic fatty liver disease.
 GeroScience doi:10.1007/s11357-023-00903-5.
- Yazar S, Alquicira-Hernandez J, Wing K, Senabouth A, Gordon MG, Andersen S, Lu Q, Rowson A,
 Taylor TRP, Clarke L et al. 2022. Single-cell eQTL mapping identifies cell type-specific genetic control of autoimmune disease. *Science* 376: eabf3041.

924

925

926 927

- Yi JM, Dhir M, Van Neste L, Downing SR, Jeschke J, Glöckner SC, de Freitas Calmon M, Hooker CM, Funes JM, Boshoff C et al. 2011. Genomic and Epigenomic Integration Identifies a Prognostic Signature in Colon Cancer. *Clinical Cancer Research* 17: 1535-1545.
- Zheng SC, Breeze CE, Beck S, Teschendorff AE. 2018. Identification of differentially methylated cell types in epigenome-wide association studies. *Nat Methods* **15**: 1059-1066.



Epigenetic drift score captures directional methylation variability and links aging to transcriptional, metabolic, and genetic alterations

Xiu Fan, Qili Qian, Wenran Li, et al.

Genome Res. published online August 1, 2025 Access the most recent version at doi:10.1101/gr.280155.124

P<P Published online August 1, 2025 in advance of the print journal.

Accepted Peer-reviewed and accepted for publication but not copyedited or typeset; accepted manuscript is likely to differ from the final, published version.

Open Access Freely available online through the *Genome Research* Open Access option.

Creative Commons License This manuscript is Open Access. This article, published in *Genome Research*, is available under a Creative Commons License (Attribution-NonCommercial 4.0 International license), as described at

http://creativecommons.org/licenses/by-nc/4.0/.

Email AlertingService

Receive free email alerts when new articles cite this article - sign up in the box at the top right corner of the article or click here.



To subscribe to *Genome Research* go to: https://genome.cshlp.org/subscriptions